Geophysical Journal International

Geophys. J. Int. (2021) **225,** 530–547
Advance Access publication 2021 January 21
GJI Geomagnetism, rock magnetism and palaeomagnetism

doi: 10.1093/gji/ggaa601

Re-assessment of the depth to the base of magnetic sources (DBMS) in Australia from aeromagnetic data using the defractal method

Raj Kumar [1], A.R. Bansal, Peter G. Betts[3] and D. Ravat [4]

[1] *Shillong Geophysical Research Centre (Indian Institute of Geomagnetism Mumbai), Shillong-*793005*, India, E-mail: raj.kumar8709@gmail.com.*
[2] *CSIR-National Geophysical Research Institute. Uppal Road, Hyderabad, Telangana* -500007*, India*
[3] *School of Earth, Atmosphere, and Environment, Monash University,* 3800*, VIC, Australia*
[4] *Department of Earth and Environmental Sciences, University of Kentucky, Lexington, KY* 40506-0053*, USA*

Accepted 2020 December 10. Received 2020 December 10; in original form 2020 June 16

SUMMARY

Australia and North America are the only two continent-wide regions, currently, with the complete wavelength spectrum of magnetic anomalies that can address the much-debated issue of the existence and understanding the magnetic state of the upper mantle. The depth to the base of magnetic sources (DBMS) has been extensively investigated in Australia in previous studies, yielding differing DBMS estimates across the continent. In this contribution, we re-assess the DBMS in Australia from aeromagnetic data using the defractal method, which simultaneously estimates the DBMS and the fractal parameter of the magnetic field. We test the effect of window size on DBMS estimates for the defractal method and conclude that a window size 10 times the expected DBMS is required for the defractal method. We also demonstrate the dependence of derived spectral slopes (and thereby depths) on the size of window by comparing spectral slopes obtained from window sizes up to 1000 km. Our analysis yields DBMS estimates between 25 and 60 km over Australia and are complexly related to temperature structure, magnetic mineralogy and petrology and geological history. Deeper DBMS estimates (∼55–60 km) are obtained for the Yilgarn Craton (West Australian Craton) and the Gawler Craton (South Australian Craton). These estimates are significantly deeper than the Moho, suggesting the uppermost mantle is ferromagnetic for these cold and old cratonic regions. Shallower DBMSs of 25–35 km are obtained in the Pilbara Craton, the eastern and southern part of the Delamerian Orogen, the northwestern part of the Canning Basin, Officer, Cooper and Georgina Basins and the Tasmanides. The areas of shallower DBMS are positively correlated with high heat flow in the regions. On the other hand, regions of large concentrations of radiogenic elements associated with the major metallogenic deposits have high heat flow arising from the radiogenic heat, but deeper DBMSs, for example the eastern margin of the Gawler Craton covered by Neoproterozoic Adelaide Rift Complex, the McArthur Basin, the Pine Creek Inlier.

Key words: Magnetic anomalies: modelling and interpretation; Fourier analysis; Fractals and multifractals.

1 INTRODUCTION

The thermal structure of the continental lithosphere is influenced by the complex interplay of the ancient geological process and recent tectonic activity. Understanding the thermal architecture of a continent is important because it informs us of crustal rheology, mechanisms of deep crustal seismicity, seismic wave attenuation, and geothermal gradients. It also helps in understanding the perturbations in the geothermal gradients from tectonic influences and the distribution of heat-producing elements. The thermal structure of a region is usually obtained directly from measurements of heat flow through bore-hole temperature and thermal conductivity measurements. The bore-hole data mainly provide information about the shallow thermal anomalies but have uneven spatial distribution. Therefore, it is difficult to map the regional thermal structures from the bore-hole data especially in regions of sparse data or when bore holes are affected by hydrologic conditions. Aeromagnetic surveys provide excellent spatial resolution at multiple scales, and are cost-effective for depicting upper crustal geology and regional thermal conditions (e.g. regions of high heat flow leading to elevated Curie isotherm and vice versa). The depth to the base of magnetic sources (DBMS), often referred to as the Curie point depths, can

be estimated from spectral analysis of magnetic data and are used as a proxy for lithospheric thermal variation and constraining the tectonic evolution of a region (Tanaka *et al.* 1999; Salem *et al.* 2014). The temperature above which magnetic minerals lose their spontaneous magnetism is known as Curie temperature (580 °C for magnetite, Dunlop & Ozdemir 1997). The depth in the Earth's lithosphere where the Curie temperature occurs is known as the Curie depth or Curie-point depth (Bhattacharyya & Leu 1975). The DBMS may, however, be a temperature as well as compositional boundary between the magnetic and non-magnetic lithosphere, as estimates of the DBMS are influenced by ferromagnetic minerals such as magnetite, titanomagnetite, hematite, pyrrhotite or native iron/iron-alloys, all having different Curie temperatures. Thus, the DBMS may be considered a temperature or a compositional boundary between the magnetic and non-magnetic lithosphere.

Estimating the DBMS is a challenging task. Different estimation methods and parameters used in the estimation, if not chosen with adequate precautions, can result in significantly different values. Chopping & Kennett (2015) and Li *et al.* (2017) calculated the DBMS in Australia for fractal source distribution using different spectral approaches and their results are very different (Figs 1a and b). Chopping & Kennett (2015) used an automatic method based on the Maus *et al.* (1997) and Bouligand *et al.* (2009) approach and estimated the DBMS using the fit of observed and modelled spectra. They stabilized the low wavenumber part of their spectra using spectra from overlapping windows and obtained depths from ensembles of solutions over a region where depths are weighted by inverse misfit to the average of logarithm of power spectrum. Li *et al.* (2017) used the modified centroid method with smaller spatial windows (∼100–300 km). We investigate, in this paper, whether such small windows, without stabilizing long-wavelengths, are capable of detecting deep DBMSs (by comparing derived spectral slopes, and thereby depths, from different window sizes).

Recently, Olsen *et al.* (2017) published the LCS-1 model, which is a global model of Earth's lithospheric field based on magnetic observations collected by the CHAMP and Swarm satellite missions. They used the Australian aeromagnetic data to substantiate the wavelength content of LCS-1 model because this continent has modern aeromagnetic observations and contain the entire spectrum of wavelengths for estimation of shallow and deep depths of anomalous magnetic bodies. The LCS-1 model does not have reliable wavelengths <250 km all over Australia and moreover disentangling the depth extent of magnetization and variation of magnetic properties is not readily possible without knowing one or the other.

We use the defractal method (Salem *et al.* 2014; Ravat *et al.* 2016) to estimate the DBMS from high-resolution aeromagnetic data of Australia. The defractal method is based on the consistency of results from the defractal centroid and the defractal spectral peak modelling. The method simultaneously leads to an estimate of the fractal parameter of the magnetic anomaly field and depths. An advantage of this method is that has fewer assumptions. The spectral method undertaken in this study are used to determine the DBMS and to understand magnetization variation within the Australian continent. We then interpret the estimated DBMS in detail in terms of geology and tectonics of the region in the context of Moho and available heat flow data and address if the Australian continental upper mantle can be magnetic or not (Wasilewski *et al.* 1979; Wasilewski & Mayhew 1992; Ferré *et al.* 2014). Ravat (2019) demonstrated that in the Archean eastern Superior Craton, North America (see also Ferré *et al.* 2020), the base of magnetization is well within the mantle.

2 BACKGROUND OF THE METHODS FOR ESTIMATING THE DBMS

In the Fourier domain, there are several approaches used for estimating the DBMS from the power/amplitude spectra of the 2-D magnetic anomaly for random and uncorrelated distribution of magnetic sources (Bhattacharyya & Leu 1975) and scaling/fractal distribution of magnetic sources (Maus *et al.* 1997). Methods used to calculate the DBMS include: the modelling of the spectral peak (Ross *et al.* 2006; Ravat *et al.* 2007); the centroid method (Bhattacharyya & Leu 1977; Okubo *et al.* 1985); the combined centroid and matched filtering (Guimaraes *et al.* 2014); the modelling of fractal magnetization (Bouligand *et al.* 2009; De Ritis *et al.* 2013); the modified centroid method (Bansal *et al.* 2011) and the defractal method (Salem *et al.* 2014).

The theoretical 2-D amplitude spectra of the total observed magnetic field (A_t) for random and uncorrelated distribution of magnetization can be written as a function of magnetization amplitude spectra (A_m), top depth (Z_t) and bottom depth (Z_b) of the anomalous magnetic body (Blakely 1995),

$$A_t\left(k_x, k_y\right) = C\left(k_x, k_y\right) A_m\left(k_x, k_y\right), \tag{1}$$

where C is the proportionality constant. This constant depends on the directions of magnetization and geomagnetic field, k_x and k_y are the wavenumbers in the x and y directions and $k = \sqrt{k_x^2 + k_y^2}$ in rad km^{-1}.

It is important to recognize that, in the theoretical expression, all linear segments of the spectra are related to the depths of some apparent magnetic horizon. The top depths can be estimated from the slopes of middle to high wavenumbers of the annular average of the natural log (ln) of the amplitude spectra of the observed magnetic field as,

$$\overline{ln(A_t(k))} = C_1 - kZ_t, \tag{2}$$

where C_1 is a constant.

Bhattacharyya & Leu (1975, 1977) proposed the centroid method for the estimation of centroid depth of a parallele-piped source with uniform magnetization. The method was later modified for a random and uncorrelated source distribution (Okubo *et al.* 1985; Tanaka *et al.* 1999). The centroid depth can be calculated from the slope of the low wavenumber segment of the annular average of the natural log of a wavenumber scaled amplitude spectra as,

$$In\left(\acute{A}_t(k)\right) - ln(k) = C_2 - kZ_0, \tag{3}$$

where C_2 is a constant and Z_0 is the centroid depth.

The DBMS (Z_b) can be estimated from the top and the centroid depths as,

$$Z_b = 2Z_0 - Z_t. \tag{4}$$

If magnetization is fractally distributed (Pilkington & Todoeschuck 1993) or if the sources are ensembles (Spector & Grant 1970), then there is an additional factor dependent of the wavenumbers that reduces the depth estimates (Maus & Dimri 1996; Fedi *et al.* 1997).

For these cases, the observed amplitude spectra ($A_o(k_x, k_y)$) can be written in terms of multiplication of random amplitude spectra ($A_r(k_x, k_y)$) and $k^{-\alpha}$ by assuming fractal magnetization (Salem *et al.* 2014),

$$A_o\left(k_x, k_y\right) = A_r\left(k_x, k_y\right) k^{-\alpha}, \tag{5}$$

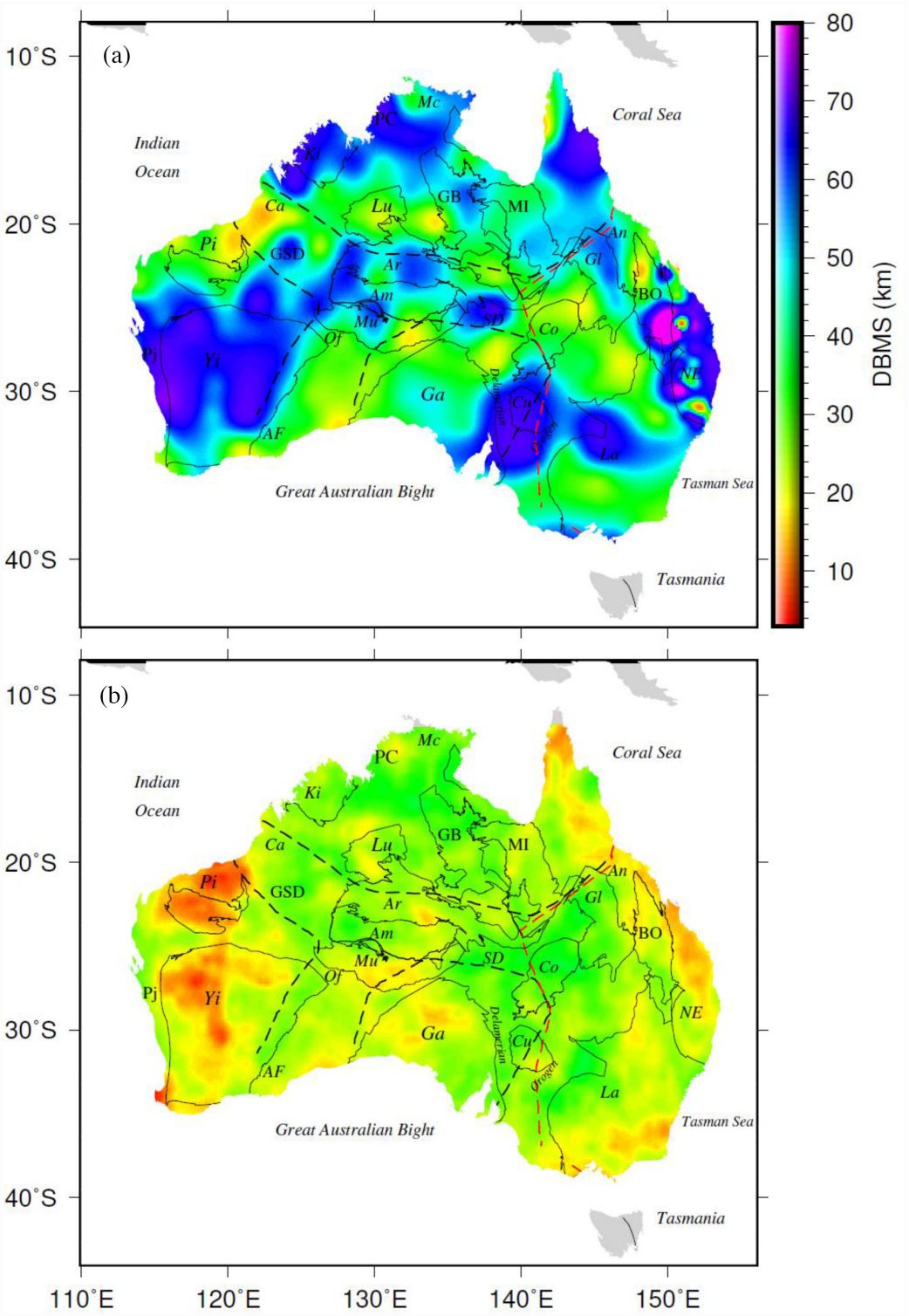

Figure 1. Maps of the depth to the base of magnetization (DBMS) values estimated by (a) Chopping & Kennett (2015) and (b) Li *et al.* (2017). As discussed in the text, there are significant differences in the DBMS derived between the two studies. The black dashed lines are used to divide the region into four parts (west, south, central, north Australia), and the red dashed line is the Tasman line delimiting eastern Australia. AF, Albany-Fraser belt; An, Anakie province; AP, Arnhem province; Ar, Arunta Inlier; Am, Amadeus Basin; Bo, Bowen Basin; Ca, Canning Basin; Co, Cooper Basin; Cu, Curnamona Province; EB, Earaheedy Basin; Ga, Gawler Craton; GB, Georgina Basin; Gl, Galilee Basin; GSD, Great Sandy Desert; Ki, Kimberley Craton; La, Lachlan Orogen; Lu, Lucas Craton; Mc, MacArthur Basin; MI, Mt Isa Inlier; Mu, Musgrave Block; NE, New England Orogen; Of, Officer Basin; PC, Pine Creek Inlier; Pi, Pilbara Craton; Pj, Pinjarra Orogen; SD, Simpson Desert; Yi, Yilgarn Craton.

where α is the fractal parameter/index of the field, which is related to the fractal parameter of magnetization $\beta \cong \alpha + 1$ (Maus & Dimri 1994). In multifractal cases, this relationship may not hold. Eq. (5) is also used frequently for correcting the power spectra for scaling distribution of sources (Fedi *et al.* 1997; Ravat *et al.* 2007; Bansal *et al.* 2011).

In the defractal method (Salem *et al.* 2014), the effect of fractal behaviour is estimated by deriving the fractal parameter of the field and removed from the observed spectra. Thus, eq. (5) can be defractalized by using a fractal index of the field, α,

$$A_r\left(k_x, k_y\right) = A_o\left(k_x, k_y\right) k^{\alpha}. \quad (6)$$

The main advantage of the defractal method is that it does not require any *a priori* information about α. In the defractal approach, α is varied until the consistency of results is obtained from the spectral peak modelling and centroid methods. Depth estimates can be achieved by selecting the wavenumber range *a priori* (e.g. Li *et al.* 2013, 2017), which may or may not fit appropriately the observed spectra, or by selecting a wavenumber range based on the observed slope for the respective window (e.g. Bansal *et al.* 2011, 2016; Ravat *et al.* 2016; Kumar *et al.* 2018, 2020).

We tested the method on a 2-D synthetic magnetic field generated from a 3-D fractal magnetization distribution (Pilkington & Todoeschuck 1993) at 1 km of elevation with the assumed parameters of 0 km top depth, 40 km bottom depth and fractal parameter of magnetization, $\beta = 3$ which results in the fractal parameter of the field, $\alpha \sim 2$ ($\alpha \cong \beta - 1$; Pilkington & Todoeschuck 1993; Maus & Dimri 1994). Pilkington & Todoeschuck (2004) further explored the relation between density from the bore-holes and 2-D gravity field observations and found that Maus & Dimri (1994) relation of $\alpha \cong \beta - 1$ is in good agreement also for density. The synthetic magnetic field along with spectra showing calculated parameters are presented in Fig. 2. Ravat *et al.* (2016) determined that large window sizes were needed to model deep DBMS using the defractal method (approximately 10 times the expected DBMS). We studied the effect of the window size in the estimation of the DBMS using the defractal method on synthetic data (Fig. 3). The window sizes of <500 km tend to underestimate the DBMS significantly. After introducing the Australian data set, we show the slopes of spectra in the low wavenumber range for one of the locations with deep DBMSs, for window sizes ranging from 100 to 1000 km. Slopes from window sizes up to 300 km are much smaller than the slopes from window sizes from 500 to 1000 km, which corroborates the results from this model study.

3 AUSTRALIAN AEROMAGNETIC DATA

There is excellent spatial coverage of geophysical data across Australia. In the past 25 yr, a number of seismic tomography studies (Debayle *et al.* 2005; Fishwick *et al.* 2008) and vast amounts of seismic reflection (Goleby *et al.* 2004; Cayley *et al.* 2011), gravity (Aitken 2010; Aitken *et al.* 2013), heat flow (Cull 1982; Cull & Beardsmore 1992; Gerner & Holgate 2010; Kirkby & Gerner 2013) and aeromagnetic data (Milligan *et al.* 2009, Milligan *et al.* 2010; Spampinato *et al.* 2015a) have been collected. We use the 6th edition aeromagnetic data of composite total magnetic intensity (TMI) grid map of Australia (Fig. 4), which is a grid of ~800 merged surveys with line-spacing less than 400 m and average ground clearance of ~80 m. The final TMI map has a grid cell spacing of ~3 s of arc or ~80 m (Milligan *et al.* 2009, 2010).

To demonstrate the need for larger window sizes to have appropriate wavelengths to estimate deeper depths, we use the example of the Yilgarn Craton region from the aeromagnetic map (Fig. 4). We chose the Yilgarn Craton because this is one of the regions where we expect deep DBMSs and the craton is also sufficiently wide to contain large window sizes up to 1000 km. Even though the spectra are mildly noisy, which is generally reduced by tapering in the actual processing, we have purposefully not modified the annular averages to avoid the effects of any processing in this demonstration. Instead, we note that the slopes of amplitude/power spectra are proportional to depths (eqs 2 and 3) and thus smaller slopes in any wavenumber range would imply smaller depths and the steeper ones would imply the deeper depths. Fig. 5 shows spectra from windows from 100 to 1000 km widths with a common centre in the middle of the Yilgarn Craton. Because the information about the centroids is in the low wavenumbers, we have computed slopes of straight-appearing low-wavenumber segments. The slopes for windows of ≥500 km × 500 km are in the similar range and steep, whereas the slopes from 100 to 300 km windows are much smaller. Thus, the depths computed from the small windows are much shallower than the depths from ≥500 km windows.

We attempted to place windows over single geological domains and blocks with magnetically cohesive patterns rather than determining the DBMS estimates at a certain grid spacing that may cover more than one geological domain. For older, colder and extensive geological elements such as the Yilgarn Craton and the Gawler Craton, the DBMS could be deeper. To ensure the deepest information we selected 1000 km × 1000 km window for larger cratonic elements and use 500 km × 500 km window for smaller geological provinces and domains (Fig. 4). We note that if the true DBMS in the region is much deeper than 50 km, our estimates may have to be considered minimum estimates. However, they should be able to discriminate between the results of previous studies. Furthermore, larger windows spanning over two different geological provinces of different DBMS does not offer any particular interpretational advantage. We determined a few different estimates by moving the windows to nearby locations and found that solutions are within ~10 per cent of each other. An example of depth and fractal parameter estimations in parts of Australia (e.g. Arunta Inlier, Yilgarn Craton, Gawler Craton and Cooper Basin) are presented in the Fig. 6.

4 THE DBMS RESULTS AND THE GEOLOGY OF AUSTRALIA

To compare our results to geology, we separate the Australian Continent into five geological domains. Three of these correspond with the Archean to Proterozoic (i) North, (ii) South and (iii) West Australia cratons similar to that defined by Myers *et al.* (1996), (iv) a central Proterozoic Domain, termed the Diamantina terrane (Cawood & Korsch 2008) and (v) the Phanerozoic Tasmanides (Cawood 2005), which comprise the eastern third of the continent (Fig. 7). Detailed interpretation of the derived DBMS in each geological province and its implication with available heat flow data and Moho depths are presented below.

4.1 WESTERN AUSTRALIA

The West Australia Craton comprises two Archean cratons, the Yilgarn and Pilbara cratons (Fig. 7), which are separated by the Palaeoproterozoic Capricorn Orogen. In the Yilgarn Craton, we calculated DBMS at two principal locations (Fig. 4) where the

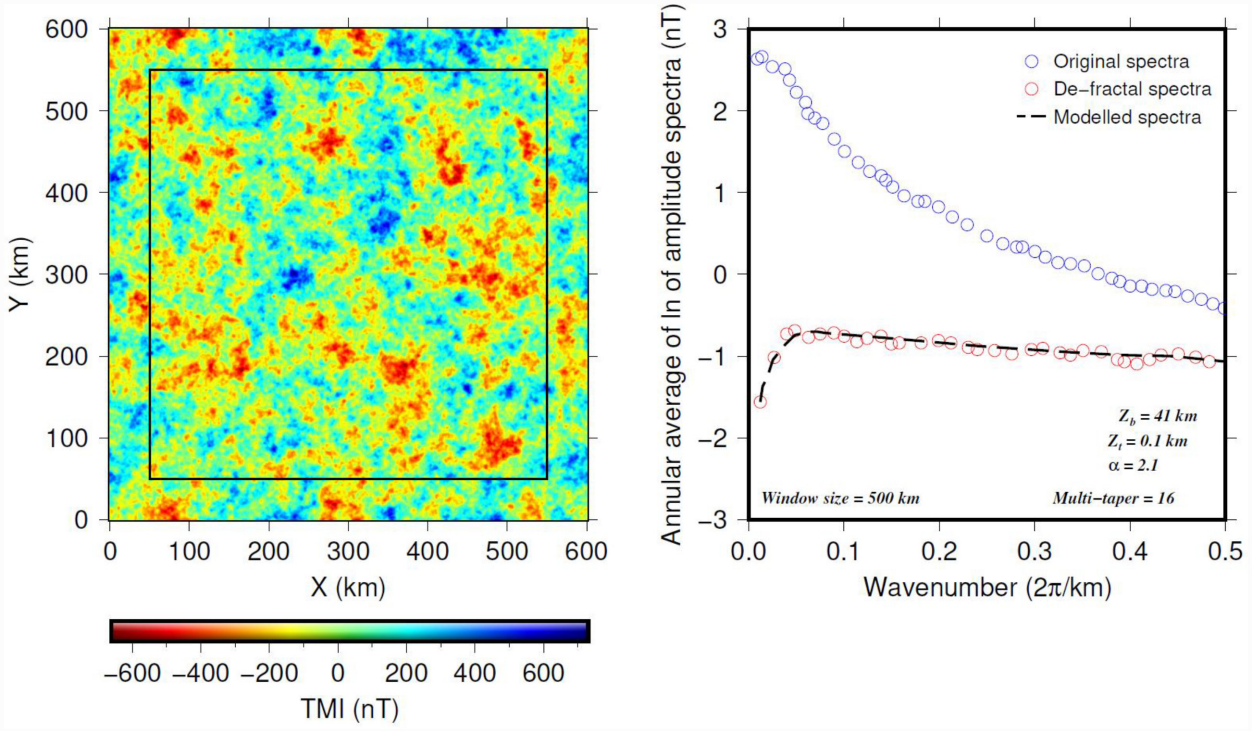

Figure 2. Left-hand panel: a synthetic 2-D magnetic field generated at 1 km elevation using 3-D fractal magnetization ($\beta = 3$) from a 600 km × 600 km × 600 km model block. The field is computed from the model with the top depth of 0 km and the bottom depth is truncated at 40 km. Because the model dimensions are restricted to 600 km, the fields calculated within about 50 km of the edges have edge effects and are not used. The model size is restricted by computational capability. The blue circle, red circle and black dashed line are the original spectra, defractal spectra and modelled spectra, respectively. The original spectra are defractaled and wavenumber-scaled for centroid depth estimation. Derived parameters: Z_t is depth to top (km), Z_b is depth to bottom (km), α = fractal parameter of the field. Multitaper stands for total number of 2-D multitapers used and Window size is one side of a square data window used in the determination.

DBMS values of 60 km and 54 km were estimated for the window sizes of 1000 km × 1000 km and 500 km × 500 km, respectively (Fig. 7; Table 1). Both these estimates are within 10 per cent of each other. Our result is closer to the estimate of Chopping & Kennett (2015) and significantly deeper than the estimates of Li *et al.* (2017), who used a fixed fractal parameter of the field ($\alpha = 2$) and smaller window sizes that have only limited sensitivity to lower crustal and mantle depths. The fractal parameter of magnetization of Chopping & Kennett (2015) is also consistent with our independently derived fractal parameter (Table 1).

The DBMS values of 54–60 km in the Yilgarn Craton are consistent with average lower heat flow in the western region of the order of 39–40 mW m^{-2} (Cull 1982; McLaren *et al.* 2003). However, the Darling Ranges granites near the western edge of the Yilgarn Craton are known as a source of radioactive heat generation (Middleton 2013). Here, the temperatures are between 60 and 110 °C at depths of 3–4 km depending on the thickness of granites. Our estimated deeper DBMS within the mantle suggests that the high geothermal gradient found at shallow depth may not be representative of the deeper crust and is primarily associated with granites. The north-eastern part of the Yilgarn Craton is characterized by the Moho depth of ∼50 km, whereas the southwestern and southern parts have Moho depths between ∼30 and 35 km. Generally, the Moho depths in the Yilgarn Craton are 35–40 km (Salmon *et al.* 2013; Fig. 8). Our estimated DBMSs of the order of 54–60 km in the Yilgarn Craton are approximately 20 km deeper than the Moho.

The Mesoproterozoic Albany–Fraser Province along the south and southeast margin of the Yilgarn Craton consists of mainly orthogneiss and granite rocks, a remnant of two extensive basins (e.g. Barren and Arid basins: Spaggiari *et al.* 2014). We estimated the DBMS of 37–45 km across the Albany-Fraser Orogen (Fig. 7, Table 1). Recently, Sippl *et al.* (2017) estimated slightly deeper Moho (∼45–51.5 km) for the Albany–Fraser Province, whereas the earlier studies had suggested shallower Moho ∼28–34 km (Clitheroe *et al.* 2000). The Albany–Fraser Province region has Mesoproterozoic underplating in the lower crust (Sippl *et al.* 2017). The lack of knowledge of magnetic mineralogy of the underplated crust and the range of DBMS values overlapping these Moho estimates makes it difficult to invoke ferromagnetic mantle in this region.

The Perth Basin and the underlying Pinjarra Orogen record a complicated history during the Palaeozoic to the Mesozoic which is characterized by obliquely oriented extensional rift system on the southwest continental margin of Australia (Holzrichter *et al.* 2014). The DBMS value of 53 km is estimated in the Perth Basin. The width of Perth Basin is ∼100 km and our window extends beyond the limits of the geological domain (and thus the estimates could be affected by the deeper DBMS from the Yilgarn Craton). The Moho depths in the Perth Basin is characterized by large lateral variations between ∼20 and 34 km with an average of 30 km (Holzrichter *et al.* 2014), whereas the DBMS value of 53 km is deeper and lies within the mantle.

The Pilbara craton is dominated by granite-greenstone lithological associations (Barley *et al.* 1998). Banded Iron Formations of the Hamersley Basin were deposited in a divergent setting along the southern margin of the Pilbara Craton at the Archean-Proterozoic

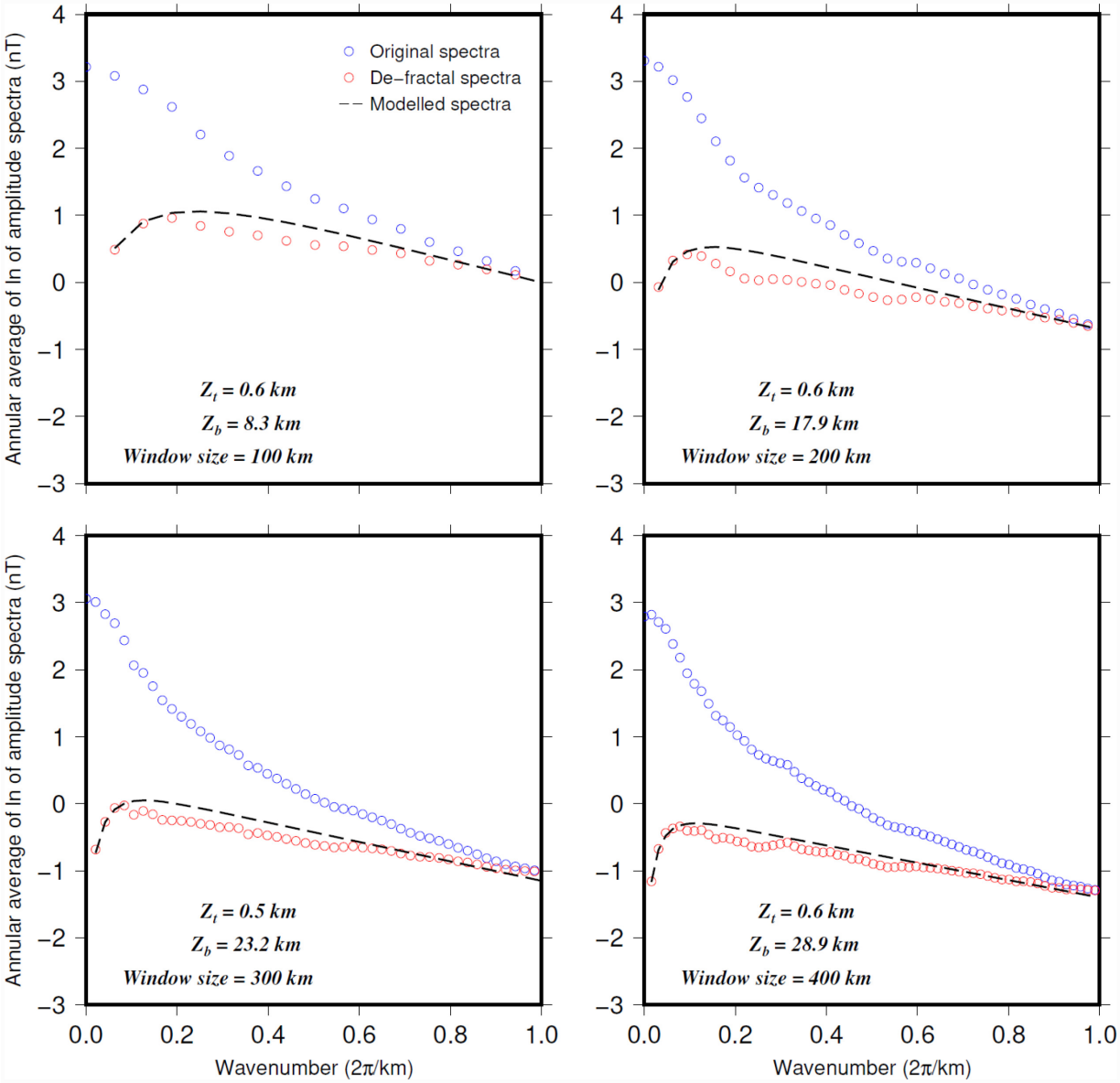

Figure 3. The depth to the top and DBMS estimates for different window sizes at fix $\alpha = 2$ and Multitaper of 16 using the defractal method. The synthetic data used for this experiment is described in Fig. 2 and the centre of all windows is (300 km, 300 km). As the window size is increased, the peak location, which is based on the DBMS, moves to lower wavenumbers. Different fits to the depth to the top will change results somewhat but because the derived tops are already shallower than 1 km, none would increase the given derived DBMS by more than 2 km and thus the derived DBMSs from these small windows will significantly underestimate the true DBMS used in the model study.

boundary (Martin *et al.* 1998) and are overlain by Palaeoproterozoic foreland basin sediments (Powell *et al.* 1999). The Rudall Complex defines the northeastern margin of the Pilbara Craton and records the Proterozoic collision of the West and North Australian cratons (Smithies & Bagas 1997; Betts & Giles 2006). In the Pilbara Craton, we estimate DBMS of 30 km (Fig. 7). The Moho depths in the Pilbara Craton are ∼30–35 km (Salmon *et al.* 2013), and thus are similar to the estimated DBMS. The heat flow in the region is low to average (Fig. 8) and consistent with its Archean-Proterozoic geology and the mantle is not likely ferromagnetic in this region. In general, there was significant variation in the DBMS values throughout the West Australian Craton and surrounding geological provinces. Beneath the Pilbara Craton, the DBMS is similar to the Moho depth, whereas in the Yilgarn Craton and southwest part of the Albany–Fraser Province the DBMSs are deeper than the Moho.

4.2 SOUTH AUSTRALIAN CRATON

The South Australian Craton consists of the Archean to Proterozoic Gawler Craton (Hand *et al.* 2007) and the Proterozoic Curnamona Province (Conor & Priess 2008), which are separated by the Neoproterozoic to Palaeozoic Adelaide Rift Zone (Powell *et al.* 1994; Priess 2000). The region has been extensively overprinted during the Cambrian-Ordovician Delamerian Orogen (Foden *et al.* 2006). Knowledge of this complex evolution of South Australian Craton is important for understanding the complexities of the DBMS variation in the region. The Gawler Craton comprises a Mesoarchean to Neoarchean core (Hand *et al.* 2007), which was accreted onto the margin of Australia during the Palaeoproterozoic amalgamation of the Nuna Supercontinent (Betts *et al.* 2016). During the late Palaeoproterozoic, the Gawler Craton occupied a proximal position

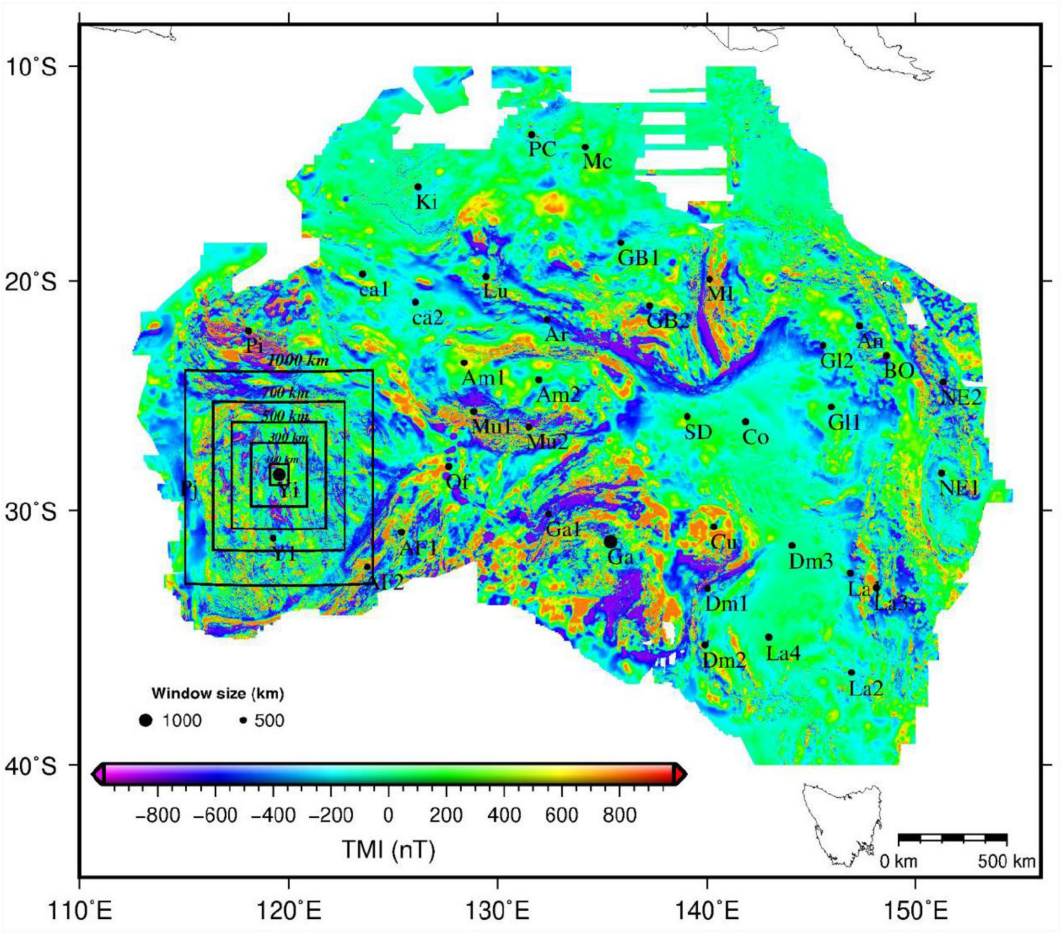

Figure 4. Aeromagnetic data over Australia (Milligan *et al.* 2009, 2010; Percival 2014). The larger and smaller circles at the centre of the location of the selected blocks of dimension of 1000 km × 1000 km and 500 km × 500 km, respectively. The window size of 100 km × 100 km, 300 km × 300 km, 500 km × 500 km, 700 km × 700 km and 1000 km × 1000 km at centre (119.55°E, 28.49°S) are presented. The abbreviations are described in Fig. 1 for geological units.

to a plate margin (Betts *et al.* 2008), recording multiple episodes of back-arc extension and magmatism (Reid *et al.* 2008), several orogenic cycles (Stewart & Betts 2010), and arc magmatism (Swain *et al.* 2008). During the Mesoproterozoic, tectonic activity shifted to the south, characterized by series of backward stepping arc terranes and oceanic rocks that are preserved in the Coompana Block, Forrest Province and the Madura Province to the west of the Gawler Craton (Spaggiari *et al.* 2015). The terranes are overlain by the Neoproterozoic Officer Basin (Cawood & Korsch 2008). The granites, felsic volcanics and gneisses in the region contain a high concentration of uranium and thorium (Houseman *et al.* 1989; Neumann *et al.* 2000) which is relevant for understanding heat flow and interpreting the DBMS in the South Australian Craton.

In the Gawler Craton, we determined DBMSs of 57 km and 48 km for window sizes of 1000 km × 1000 km and 500 km × 500 km, respectively (Fig. 7). The crustal thickness of the South Australian Craton varies from 30 to 45 km. Crust thicker than 40 km occurs in the Archean Gawler Craton and Curnamona Province (Clitheroe *et al.* 2000; Kennett *et al.* 2011). The northwestern margin of the Gawler Craton is covered with the sedimentary rock of the eastern Officer Basin and has the Moho depth of ∼40–45 km (Salmon *et al.* 2013). The eastern margin of the Gawler Craton is covered by the Neoproterozoic Adelaide Rift Complex. This complex has been subsequently shortened during the Cambrian-Ordovician Delamerian Orogen and has the Moho depth of 30–40 km (Clitheroe *et al.* 2000).

The Curnamona Province is characterized by a moderate DBMS of 39 km. The Curnamona Province and the southwestern part of the Delamerian Orogen (at the eastern boundary of Gawler Craton) is characterized by the high heat flow of the order of ∼110–150 mW/m^2 (Fig. 8), which is associated with near surface high radiogenic element concentrations within Proterozoic granite and granite gneisses, but the deeper temperatures must be much lower and consistent with its age (McLaren *et al.* 2006). This results in a complex magnetic structure of the lithosphere and the derived DBMSs likely reflect deep crustal/upper mantle temperatures.

4.3 CENTRAL AUSTRALIA

The central Australian terranes comprise a complex mosaic of Palaeo- to Mesoproterozoic basement rocks with intervening stacked basins that evolved during the Neoproterozoic to the recent history. The basement terranes include the Arunta Inlier (or Aileron Province), which accreted along the southern margin of the North Australia Craton ca. 1850 Ma during the Nuna Supercontinent

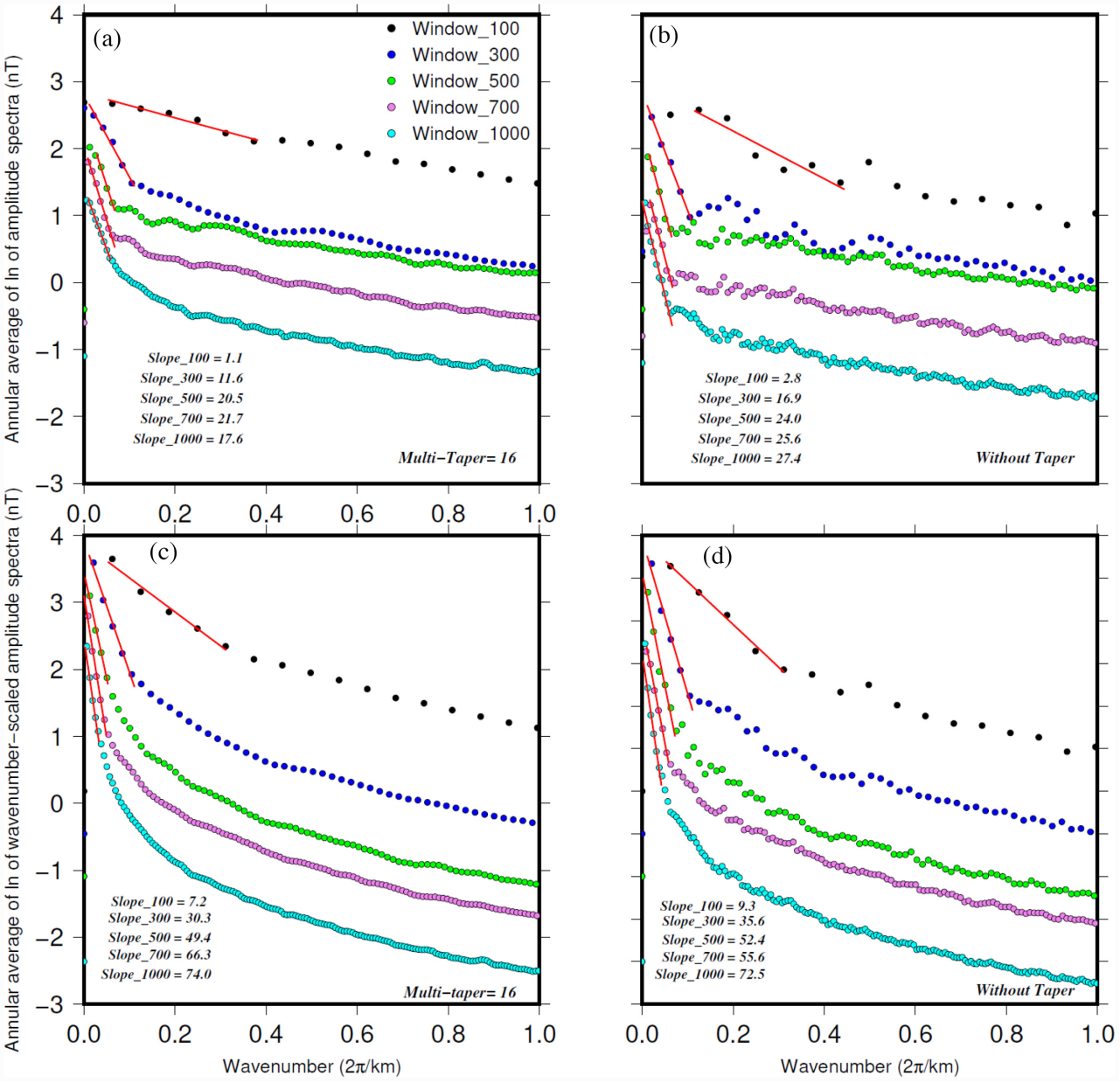

Figure 5. Low wavenumber range slopes from the spectra calculated from the Yilgarn Craton windows shown in Fig. 4 demonstrating that small windows lead to smaller slopes and thus smaller depth estimates. See text for details. (a, b) unmodified low wavenumber range slopes of amplitude spectra for different window sizes with multitapers and without tapers, and (c, d) wavenumber-scaled low wavenumber range slopes with multitapers and without tapers, that would be used in the centroid depth calculations. Parts (a) and (c) are only for illustration of how slopes change between the amplitude spectra and the wavenumber-scaled spectra.

amalgamation (Betts *et al.* 2016). The Arunta Inlier records a complex evolution of Palaeo-Proterozoic to Mesoproterozoic tectonic reworking along the southern margin of the Australian continent (Betts & Giles 2006; Morrissey *et al.* 2014), leading to the amalgamation of the Rodinia Supercontinent.

The Musgrave Block, to the south, records a protracted evolution of Mesoproterozoic juvenile arc magmatism at the southern margin of the Australian plate (Wade *et al.* 2006), which was subsequently deformed during the late Mesoproterozoic Musgravian Orogeny and coincident with the pervasive magmas of the Pitjantjatjara Supersuite (Kirkland *et al.* 2013). Following the Musgravian Orogeny the western Musgrave Block and regions to the west were extensively overprinted by the Warakurna Large Igneous Province (Pirajno & Hoatson 2012), leading to the onset of the development of the Centralian Superbasin, which includes the Eucla, Ngalia, Amadeus, Savory, and Georgina basins (Maidment *et al.* 2007).

The DBMS in central Australia varies between 31 and 48 km (Fig. 7, Table 1). The DBMS is shallower (35 km) in the northern Canning Basin and the eastern central Officer Basin. It is moderate (42–48 km) along an NNE-trending crystalline basement ridge extending from Musgrave Block, Amadeus Basin, and Arunta Inlier (Aitken & Betts 2008). The Moho depth in the most of central Australia ranges is highly variable (~30–50 km, and greater in a few places) and is influenced by intraplate Orogenesis (Aitken *et al.* 2009; Kennett *et al.* 2011). In the Musgrave Block, the crustal thickness ranges from 25–50 km (Aitken *et al.* 2009) with a transitional

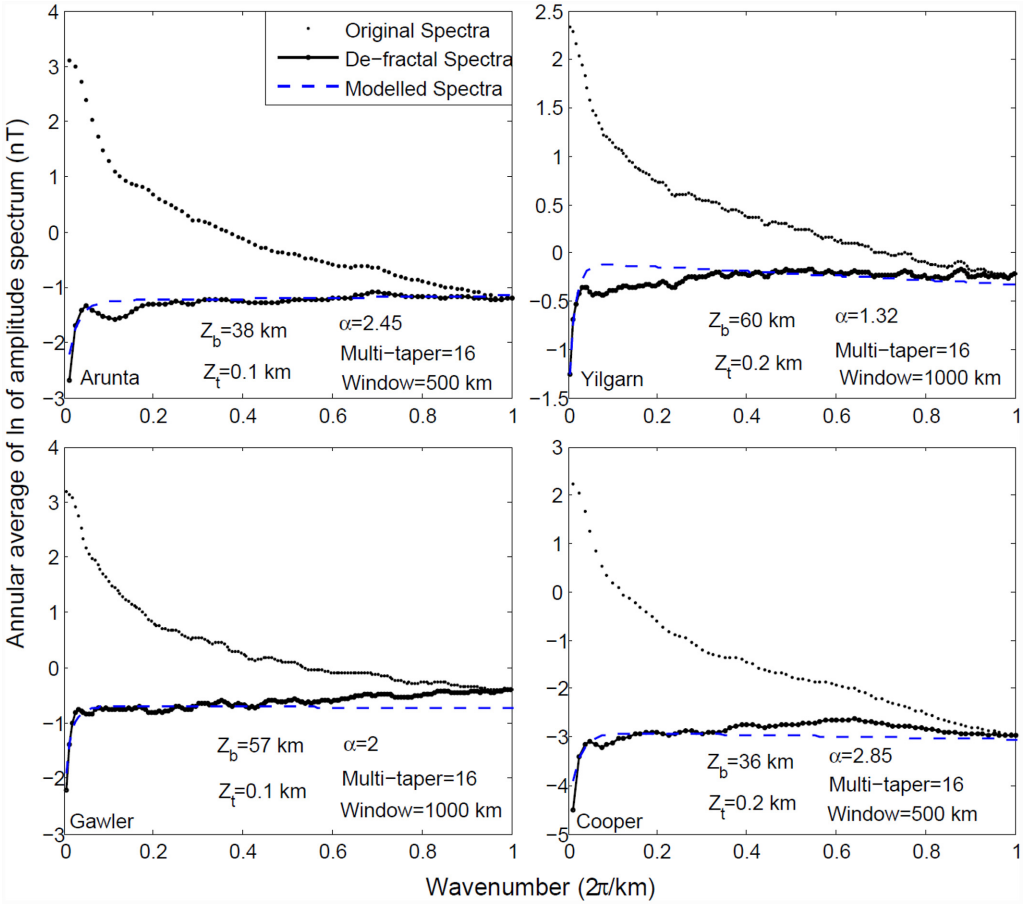

Figure 6. Plot of annular averages of natural logarithm of amplitude spectrum versus wavenumber showing the defractal DBMS estimates for Arunta block, Yilgarn Craton, Gawler Craton and Cooper basin. Derived parameters: Z_t is depth to top (km), Z_b is depth to bottom (km), α = fractal parameter of the field.

crust-mantle boundary which similarly extends to the South Australian Craton. The crustal thickness beneath the Arunta Inlier is variable with a depth of 35–40 km and 50 km in the north and the south of the inlier (Goleby *et al.* 1989). The region has mantle material at a depth between 25–30 km indicating significant thrusting (Goleby *et al.* 1989, 1990). The mid-crust high density and high velocity material is also found from other geophysical studies beneath the Central Arunta block (Lambeck 1983; Lambeck *et al.* 1988). The Amadeus Basin has Moho depths of ∼60 km based on gravity and seismological modeling (Goleby *et al.* 1989). The Moho depth of 30–35 km occurs beneath the Canning Basin (Salmon *et al.* 2013). The estimated DBMS are found shallower than the Moho by about 10–20 km in the Arunta Block, Amadeus Basin, and Musgrave Block. There are very few heat flow data in central Australia which varies from 31–68 mW/m^2.

4.4 NORTHERN AUSTRALIA

The North Australian Craton comprises the Kimberley Craton, the Pine Creek Inlier, the Arnhem Province, Granites-Tanami Block, the Mt Isa Inlier, Greater McArthur Basin, Tennant Creek-Davenport Province, and the Georgetown Inlier (Withnall *et al.* 2013). The geological evolution of the North Australia Craton is dominated by Palaeoproterozoic and Mesoproterozoic tectonic events, although the basement is interpreted as Archean. The craton is extensively overlain by younger Neoproterozoic to Palaeozoic basins.

The tectonic evolution of northern Australia records a series of accretionary events between 1860 Ma and 1600 Ma, when Arunta Inlier, Gawler Craton, Kimberley Craton and Georgetown Inlier amalgamated with the nucleus of the North Australian Craton (Betts *et al.* 2016; Nordsvan *et al.* 2018) along subduction zones that had established along the southern, western and eastern margins of the craton. The oldest basins preserved in the Granites–Tanami Block, Arunta Inlier and the Tennant Creek–Davenport Province (Allen *et al.* 2015), which were followed by the ca. 1800–1740 Ma extensional Leichhardt Superbasin (Neumann *et al.* 2009) and the ca. 1720–1670 Ma Calvert Superbasin (Gibson *et al.* 2008). These basins are extended over a large area of the North Australia Craton and adjacent terranes (e.g. Gawler Craton and Curnamona Province) (e.g. Allen *et al.* 2015). The fourth basin cycle, the Isa Superbasin (ca. 1668–1595 Ma: Southgate *et al.* 2000) is also extensively preserved through the North Australia Craton but appears to record a post-extensional evolution (Gibson *et al.* 2018). The fifth basin cycle, the epicontinental Roper Super basin initiated ca. 1430 Ma (Jackson *et al.* 1988) and is best preserved in the Greater McArthur Basin in the northern and central North Australia Craton (Allen *et al.* 2015). Basins of the North Australian Craton have been inverted during several shortening events including the Leichhardt Event (Blaikie *et al.* 2017), Riversleigh Event (Gibson & Edwards 2020) and the Isan Orogeny (Betts *et al.* 2006).

In northern Australia, the calculated DBMS ranges between 29 and 43 km (Fig. 7, Table 1). The thickest crust of 55 km found

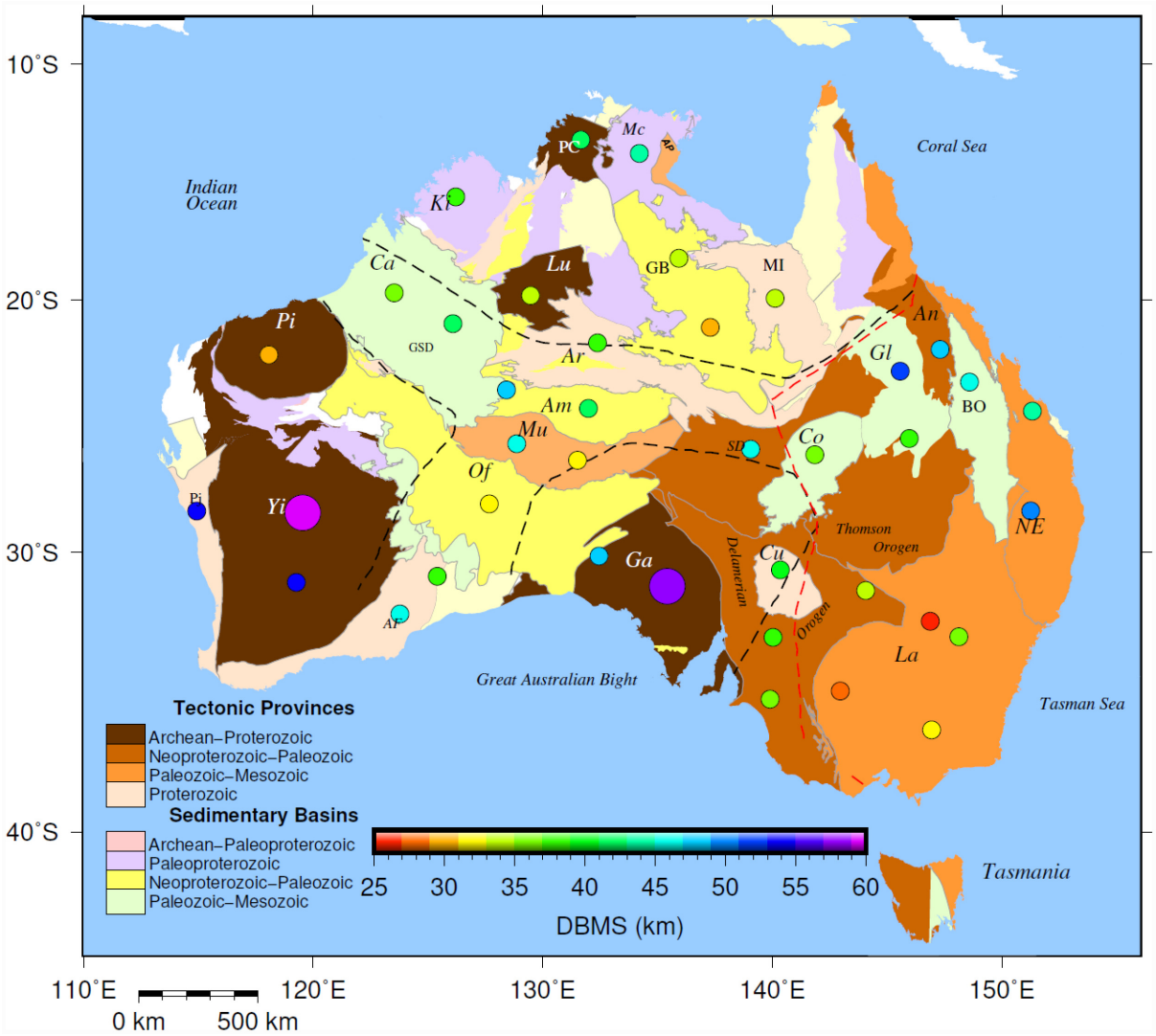

Figure 7. Simplified geological map of Australia (Stewart *et al.* 2013) superimposed with the estimated DBMS presented by coloured circles at the location described in Fig. 4. The larger circles correspond to the centre of windows of size of 1000 km × 1000 km used for calculations in Yilgarn and Gawler Cratons. Abbreviations are the same as described in Fig. 1.

in the northern Australian region beneath Mount Isa Inlier and the northern part of the Arunta inlier (Goleby *et al.* 1989). The DBMS of 43 km in the McArthur Basin is similar to the Moho depth (40–50 km) (Kennett *et al.* 2011; Salmon *et al.* 2013). The northwestern part of Northern Australia comprises Palaeoproterozoic Kimberley Craton, which has the Moho depths between 40 and 45 km, whereas the DBMS is estimated at 37 km. Both estimates are within each other's error envelopes (Figs 7 and 8).

4.5 TASMANIDES (EASTERN AUSTRALIA)

The eastern third of the Australian continent records the Phanerozoic tectonic accretion along the eastern margin of Gondwana and collectively termed the Tasmanides (Glen 2005; Rosenbaum 2018). The Tasmanides are composed of the Cambrian-Ordovician Delamerian Orogen (Foden *et al.* 2006), the Cambrian-Carboniferous Lachlan (Glen 2005) and Thomson orogens (Spampinato *et al.* 2015b), Cambrian to Carboniferous Mossman Orogen (Fergusson & Henderson 2015) and Neoproterozoic to Triassic New England Orogen (Cawood *et al.* 2011). The orogenic systems of the Tasmanides are highly contorted and form large oroclines (Cawood *et al.* 2011; Moresi *et al.* 2014). Several extensive Ordovician-Silurian arc terranes extend along the length of the Lachlan Orogen (Glen 2005), possibly into the Mossman Orogen (Fergusson *et al.* 2017).

The oldest extensional back-arc basins of the Lachlan Orogen and Thomson Orogen (overlain by Cooper Basin, Galilee Basin, Bowen Basin and eastern part of the Simpson Desert, Fig. 7) are likely to have formed as oceanic basins or on hyper-extended continental crust (Collins 2002; Collins & Richards 2008), whereas the younger backarc basins of the New England orogens formed in a continental setting (e.g. Bowen and Galilee Basins: Korsch *et al.* 2009). The Permo-Triassic Cooper Basin developed above the southern Thomson Orogen and likely formed in a distal continental backarc setting.XXX

Shallow DBMSs exist in the Neoproterozoic to Palaeozoic Lachlan Orogen (25–35 km), in the eastern and southern part of the Delamerian Orogen (33–38 km) and in the Cooper Basin (~36 km, Fig. 7, Table 1). The Moho in the Cooper Basin is ~30–35 km (Fig. 8), that is similar to the DBMS values. The Cooper Basin is

Table 1. Estimated DBMS, top depths, fractal index and selected block size of main geological provinces in Australia. The depths and fractal parameter of magnetization by the two studies (Chopping & Kennett 2015; Li *et al.* 2017) are provided for comparison.

Geological unit or location shown in Fig. 4	This study				(Chopping & Kennett 2015)		(Li *et al.* 2017)
	One side of window size (km)	DBMS (km)	Top depth (km)[a]	Fractal parameter of the field (α)	DBMS (km)	Fractal parameter of magnetization (β)[b]	DBMS (km) (At constant, $\alpha = 2$)
Western Australia							
Yilgarn Craton (Yi)	1000	60	0.2	1.32	66	2.43	15
Y1	500	54[c]	1.0	0.75	55	1.96	14
Albani-Fraser Belt							
AF1	500	37	0.4	2.15	30	2.77	23
AF2	500	45	4	2.28	37	2.33	24
Pinjara Orogen (Perth Basin)	500	53[c]	0.2	1.3	68	2.71	21
Pilbara Craton	500	30	0.2	1.32	31	2.22	10
Southern Australia							
Gawler Craton (Ga)	1000	57	0.1	2.0	43	2.85	25
Ga1	500	48	3.5	0.98	47	2.59	21
Curnamona Province	500	39	1.9	1.80	68	3.42	30
Central Australia							
Arunta Inlier	500	38	0.1	2.45	59	3.03	25
Canning Basin							
Ca1	500	35	9.6	1.15	27	3.14	24
Ca2	500	42	9.1	1.20	19	3.30	28
Musgrave Block							
Mu1	500	45	0.3	2.0	48	2.80	21
Mu2	500	31	0.7	1.85	28	2.32	17
Amadeus Basin							
Am1	500	48	4.3	2.35	62	3.28	32
Am2	500	42	5.5	1.45	48	2.67	25
Officer Basin	500	31	6.87	1.30	30	2.95	22
Simpson Desert	500	46	1.4	2.30	48	3.56	33
Northern Australia							
MacArthur Basin	500	43	1.9	2.25	57	3.39	29
Pine Creek Inlier	500	41[c]	1.6	2.45	58	3.08	18
Georgina Basin							
GB1	500	34	1.6	2.42	58	3.56	31
GB2	500	29	6.6	1.9	39	2.75	27
Mt Isa Inlier	500	34	3.0	1.7	46	2.74	24
Kimberley Craton	500	37	1.5	2.6	64	2.92	26
Lucas Craton	500	34	1.6	1.85	25	2.84	19
Eastern Australia							
Cooper Basin	500	36	0.2	2.85	30	3.51	36
Delamerian Orogen							
Dm1	500	38	3.4	1.85	48	2.98	24
Dm2	500	36	1.5	2.0	61	2.88	24
Dm3	500	33	2.7	1.68	69	2.62	35
Bowen Basin	500	46	0.9	2.10	22	2.74	19
Galilee Basin							
Gl1	500	37	5.4	1.80	56	3.75	28
Gl2	500	52	0.8	2.52	37	3.43	26
Anakie province	500	48	0.9	2.10	36	2.77	22
Lachlan Orogen							
La1	500	25	0.7	1.85	33	2.80	21
La2	500	31	3.5	1.48	58	2.65	16
La3	500	35	3.9	1.45	32	2.90	23
La4	500	28	3.4	1.48	64	2.68	28
New England Orogen							
NE1	500	50	0.4	2.1	60	1.79	24
NE2	500	44	0.6	2.10	59	1.69	14

[a]This top depth is based on one-layer model averaged over a large area and is not meaningful locally.
[b]$\alpha \cong (\beta - 1)$ (Maus & Dimri 1994), In multifractal cases, the relationship may not hold.
[c]Smaller than ideal window size result forced by the limited extent of the geological province.

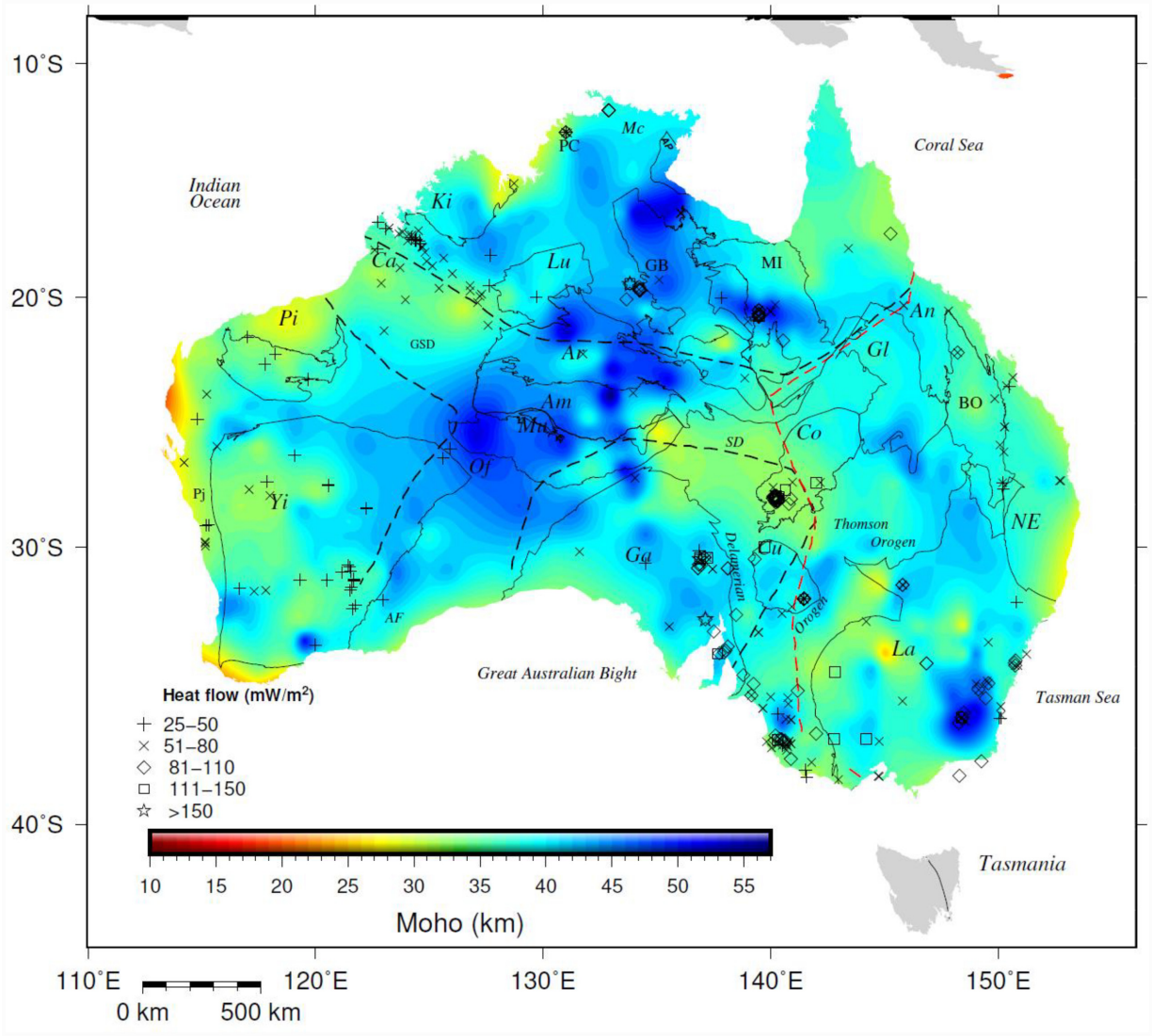

Figure 8. Moho depth map from a weighted average grid of Salmon *et al.* (2013) that reflects geological and tectonic variability of the data to some degree, superimposed with heat flow values (Kirkby & Gerner 2013) and tectonic province boundaries in Australia. The heat flow data locations and values are shown by different symbols given in the legend.

characterized by the high heat flow (∼110 mW m^{-2}) and temperatures of ∼235 °C at 5 km depth (Fig. 8; Gerner & Holgate 2010). The elevated heat flow is attributed to the high heat production from granitic rocks in the basement (Beardsmore 2004). Detailed modeling suggests that the relationship of high heat production to granites is complex (Meixner *et al.* 2012, 2014) and it is very likely that the region has more complex magnetic distribution and layering.

The Moho depth across the Tasmanides is highly variable (Clitheroe *et al.* 2000; Salmon *et al.* 2013). Fishwick *et al.* (2008) found a series of steps in the lithospheric thickness in eastern Australia from surface wave tomography and horizontal gradient of shear wave speed. The steps in the lithospheric thickness correlate with the terrane boundaries. The eastern part of the Australian continent has undergone a complex evolution during its collision with the Proterozoic shield in the late Palaeozoic. The thick crust of the order of ∼50 km is associated with the eastern Lachlan Orogen, centred beneath the eastern Australian highlands (Clitheroe *et al.* 2000). The DBMS in the Lachlan Orogen shows a general inverse correlation with heat flow. There is no correlation between the DBMS and crustal thickness (Fig. 8).

5 COMPARISON WITH THE RECENT STUDIES OF THE DBMS ESTIMATIONS

Chopping & Kennett (2015) estimated DBMS from aeromagnetic data of the Australian continent using an automated inversion scheme based on the earlier methods (Maus *et al.* 1997; Bouligand *et al.* 2009) and determined values between 10 and 80 km. Chopping & Kennett (2015) presented weighted DBMS recovered from the ensemble of calculated depths in each individual window. For weighting the depths in a window, they used an asymptotic weighing factor derived from the ensemble of solutions that fit within the statistical distribution for the averaged 1-D power spectra for that window. Their DBMSs are relatively shallow for the Cooper Basin and deep in the Yilgarn Craton, meeting the expectation based on the tectono-thermal age and heat flow (Table 1).

Li *et al.* (2017) reported shallow DBMS of the order of 5 km for the Yilgarn and Pilbara cratons, (see Fig. 1, Li *et al.* 2017), which is a surprising result for the region. Li *et al.* (2017) argue that bimodal shallow Curie depths may be possible due to deep thermal reactivation. However, the geological record of these cratons provides no

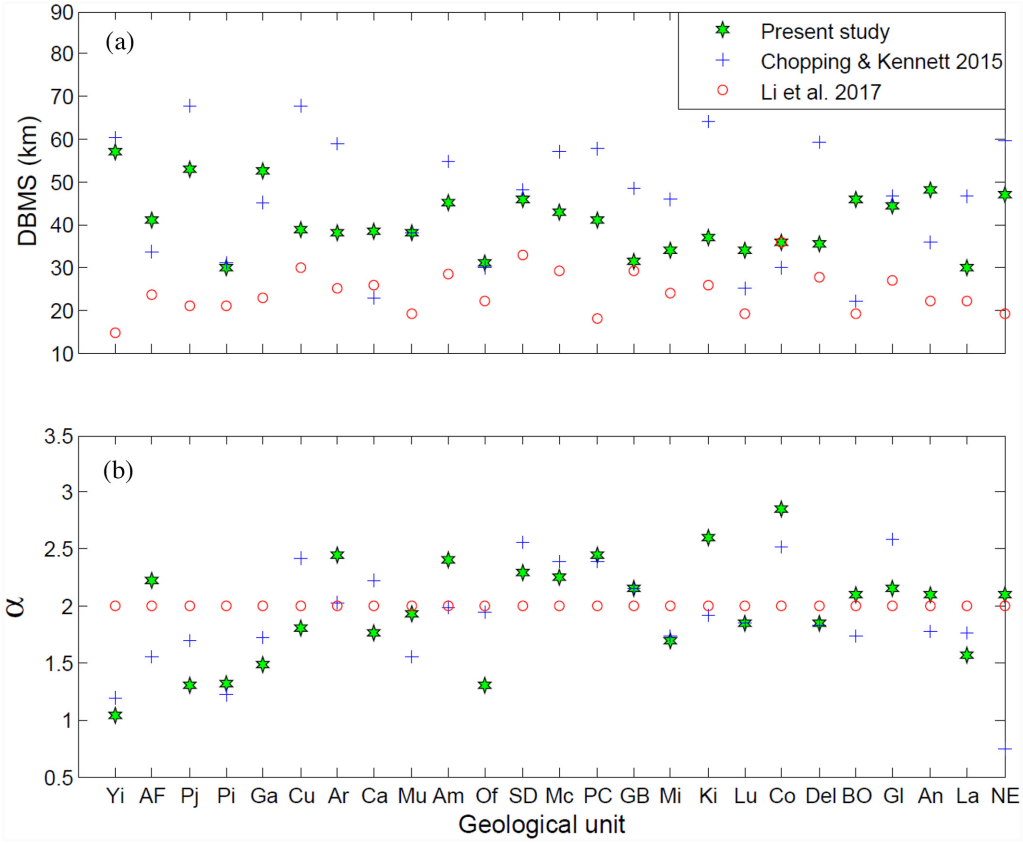

Figure 9. Comparison of the averaged estimates from different studies (a) DBMS (b) α, with geological unit of Australia. Abbreviations are the same as described in Fig. 1; Del: Delamerian Orogen.

evidence for such a craton-wide reactivation, nor does the surface heat flow data. However, Li *et al.* (2017) used a modified centroid method and fixed a value of $\alpha = 2$ with smaller window sizes of the dimension 100–300 km, which are biased towards shallow depth estimates as we demonstrated from the comparison of spectra of different window sizes in Figs 3 and 5.

In the southern Yilgarn Craton, we estimate a DBMS of 54 km and the fractal parameter of the field of $\alpha = 0.75$ (from a 500 km window), which are lower than the estimates in the central Yilgarn Craton. Chopping & Kennett (2015) have obtained DBMS of 54 km and an equivalent $\alpha \sim 0.95$ which is similar to our estimate. For the Pilbara Craton, our estimates of DBMS and α are closer to that estimated by Chopping & Kennett (2015) (Table 1, Fig. 9). In the Cooper Basin, our DBMS and α estimates are also similar to those of Chopping & Kennett (2015). Despite our α being different than Li *et al.* (2017), our DBMS estimates are near identical for the Cooper Basin. This is likely the effect of their small window size (∼100–300 km). Our estimates of the DBMS in the Tasmanides are close to the DBMS calculated by Li *et al.* (2017) where our estimated α is close to 2 (Table 1, Fig. 9). The overall shallower estimates of Li *et al.* (2017) in the region are probably a result of their small windows (∼100–300 km) and averaging over different window sizes. In the Tasmanides, Chopping & Kennett's (2015) DBMS estimates are very deep at two locations (Table 1) compared to our result, despite similarities in the derived α for both studies. Our overall smaller DBMS are consistent with the intermediate to high heat flow in the region.

In general, our estimated high values of DBMS are comparable with those determined by Chopping & Kennett (2015) for the Yilgarn Craton, Gawler Craton, Pinjara Orogen and northeast part of Australia, whereas there is a significant difference between the estimations for the eastern and southern part of Delamerian Orogen and the Tasmanides. The reason for this difference could be that their weighting scheme and smaller window sizes may not have sufficiently stabilized the low wavenumber power spectrum. Our defractal method estimates depths from the combination of centroid and spectral peak matching of the defractal spectra, whereas Chopping & Kennett (2015) used the RMS between observed and modeled spectra with a range of depths to top, base, scaling exponents.

6 DISCUSSION

There are significant differences in the DBMS estimated by Chopping & Kennett (2015) and Li *et al.* (2017) in Australia despite the high quality of aeromagnetic data. This data has significant potential to address the nature of mantle magnetization. We estimated DBMS and corresponding fractal parameters of field using the defractal method and by selecting the largest windows possible near to the centres of geological/tectonic provinces which avoids province overlap errors in the DBMS as much as possible. For large geological provinces (e.g. Yilgarn Craton, Gawler Craton, Lachlan Orogen etc., Figs 4 and 7), we also calculated DBMS at additional locations to understand the spatial variation of the DBMS within the region. We used the DBMS to understand the relationship with the Moho depth, tectono-thermal age and heat flow. Our estimated DBMS have approximately ∼10 per cent error based on nearby estimates, the ability to select correctly the low wavenumbers used in fitting

the slopes, and perhaps have larger error when the window sizes are not optimal in areas of deep magnetization. The DBMS estimates are shallower than the Moho across most of northern Australia except its northeastern part (near Coral sea), the Curnamona Craton, the central Australia, the Cooper Basin, the Lachlan Orogen and the south and east of the Delamerian Orogen. The estimates are deeper than the Moho in western Australia (except the Pilbara Craton), the Gawler Craton, the Galilee Basin, as well as for the New England Orogen, the Bowen Basin and the Anakie Province in the Eastern Tasmanides. Shallower DBMSs are consistent with high-temperatures (Gerner & Holgate 2010) and high heat flow (Fig. 8) observed from bore-hole measurements.

Early studies based on the mantle xenolith samples (Wasilewski *et al.* 1979; Wasilewski & Mayhew 1992) suggested that the seismic Moho is a magnetic boundary. The position of seismic Moho may lie below or above the compositional crust–mantle boundary (petrological Moho) based on the mineral facies changes caused by the tectonic and high geothermal gradient in the region (Mengel & Kernt 1992). The Curie temperature in the continental lithosphere may vary with its mineral composition (e.g. the increase of Ti content of titanomagnetite causes reduction in Curie temperature below 580 °C), whereas serpentinized ultramafic bodies in the upper mantle in the subduction wedges may increase Curie temperature from 620 to 1100 °C (Haggerty 1978; Blakely *et al.* 2005). However, the DBMS relationship with the Moho depth and heat flow is more complex. The seismic Moho may also not be a lithological boundary as found in electrical studies (Clitheroe *et al.* 2000). The study based on measured low heat flow revealed Curie depths of 60–70 km in southwestern Australia composed primarily of early Archean cratons (Cull 1991; Artemieva 2006). Toft & Haggerty (1988) used lower crustal xenoliths from the West African craton and petrological considerations to argue for the stability of the native iron up to the depth of 95 km. A recent review on the magnetization of the upper mantle suggests the possibility of upper mantle ferromagnetism under several conditions based on mineral and rock magnetic data, high pressure and temperature experimental results and spectral analysis of magnetic anomaly data (Ferré *et al.* 2020). Significantly deeper DBMSs than the Moho (e.g. Yilgarn Craton and Gawler Craton) indicate that the upper mantle is ferromagnetic and the seismic Moho is not a magnetic boundary (Ferré *et al.* 2014) and is consistent with recent results from North America, where DBMS estimates reveal a ferromagnetic upper mantle (Ferré *et al.* 2020). Plume impingement beneath the Australian continent and associated underplating in the past (Betts *et al.* 2002) and associated oxidation state may have played a role in changing the magnetic nature of the upper mantle.

The previous reconstructions of the Australian continent have suggested a geological correlation between the Curnamona Province (South Australian Craton), and the Mount Isa Inlier (North Australian Craton, e.g. Giles *et al.* 2004). The estimated DBMS for the Mount Isa Inlier (34 km) and Curnamona Province (39 km) are comparable. These observations suggest that the DBMS in combination with the thermal structure and the Moho depth may provide insights into the evolution of geological provinces as well as magnetic mineralogy of the deep crust and upper mantle.

The Yilgarn and Pilbara cratons have similar Moho depths despite their difference in crustal structure (Betts *et al.* 2002) and their age difference (Clitheroe *et al.* 2000). The West Australian Craton has a lower surface heat flow between 20 and 50 mW m^{-2}. Other than local variations, the heat flow values are found inversely proportional to the tectonic ages of underlying rocks from the worldwide data (Vitorello & Pollack 1980; Morgan 1985; Neumann *et al.* 2000). Therefore, deeper DBMS of the order of 50–60 km and magnetic upper mantle in the Western Australian Craton is expected. While the differences in the magnetic properties of mantle between Yilgarn and Pilbara cratons is intriguing, it is clear that very shallow DBMS obtained by Li *et al.* (2017) in all of Pilbara and large parts of Yilgarn craton appear difficult to reconcile with their geological evolution as well as geophysical data.

The Delamerian Orogen of the eastern part of Australia has been correlated with the deformed rocks preserved in the Anakie Inlier in northern Australia. Both these regions were located at the passive margin of Rodinia (Fergusson *et al.* 2009). For the Delamerian Orogen, the DBMS varies from 33 to 38 km, with the lowest values (33 km) along the eastern margin and the deepest values (38 km) along the western-central part. The DBMS in the Anakie Inlier is 48 km, deeper than the values obtained in the Delamerian Orogen. The large difference in the estimated DBMS values in the Delamerian Orogen and Anakie Inlier indicate different mineralogical and temperature conditions at depth, as well as the significant post-Ordovician tectonic overprint of the Anakie Inlier.

The Tasmanides comprise three orogenic domains (Lachlan, Thomson, and Mossman orogens) that have previously been correlated based on their similar tectonic evolution (Rosenbaum 2018). There is a large variation of the DBMS in the Tasmanides (from 25 to over 50 km). This variation is likely related to the complex tectonic overprint of this accretionary orogen and Phanerozoic, Mesozoic and Cenozoic magmatism (Jones & Verdel 2015). Additionally, eastern Australia has the longest volcanic track of 2000 km which formed between 33 and 9 Ma. This long volcanic tract has different composition depending on the lithospheric composition depending on the lithospheric thickness in the region (Davies *et al.* 2015). The volcanism in the region is seen to affect the base of magnetization, leading to the shallow DBMS in the region. For example, in the south, the Lachlan Orogen is characterized by DBMS between 25 and 35 km where the Neo-tectonic Newer Volcanic Province overprints the orogen.

Vervelidou & Thebault (2015) have determined the thickness of the magnetic layer globally using the NGDC spherical harmonic degree 720 model using spherical cap spectral analysis techniques (minimum wavelength of the model approximately 55 km but intermediate wavelengths in original surveys are not reliable over many regions of the world). However, their results are averaged over the spherical cap of >3000 km aperture. They obtain deep base of magnetization in the eastern third of North America and adjacent Atlantic Ocean, but indirectly confirm the spectral defractal method results of Ravat (2019) and Ferré *et al.* (2020). Unfortunately, in Australia where the extent of the continent is about 3000 km (i.e. most windows over the continent are averages over the continent and the surrounding oceans), thus, mixing estimates over many tectonic provinces.

7 CONCLUSIONS

Using spectral slopes from different window sizes we conclusively show that small windows lead to incorrect depths when the actual DBMSs are deeper. The results based on the defractal method show that the DBMS varies from 25 to 60 km for the whole of Australia, broadly consistent with the results of Chopping & Kennett (2015). The DBMS value ranges are 30–60 km for the West Australian Craton, 39–57 km for the South Australian Craton, 31–48 km for central Australian (Diamantina terrane), 29–43 km for the North Australian Craton and 25–52 km for the Tasmanides. Deeper DBMSs were

obtained in the Yilgarn Craton, Gawler Craton, Pinjara Orogen, the southern part of the Albany-Fraser belt. Shallower DBMS estimates were determined for the Pilbara Craton, the eastern and southern part of the Delamerian Orogen, the northwestern part of the Canning Basin, Officer Basin, Cooper Basin and in the Tasmanides. The Cenozoic magmatism has affected the DBMSs in the Tasmanides. The DBMSs significantly deeper than the Moho in the Archean cratons suggests that mantle in these regions is ferromagnetic. The base of magnetization in the Australian lithosphere is complexly related to temperature structure, magnetic mineralogy and petrology and its tectonic history.

ACKNOWLEDGEMENTS

RK is thankful to Director, SGRC (IIG Mumbai), India for permission to publish this work. RK and ARB are thankful to Director, CSIR-NGRI, India for granting permission to publish this work. We are also thankful to Prof V. P. Dimri, Dr U. K. Singh, Prof B. L. N. Kennett, Dr M. Salmon, Dr A. P. Singh, Prof M. Radhakrishna, Tony Saini and Richard Chopping for useful discussion during this study. We thank Dr V. K. Rao, Dr S. P. Anand, and Dr Eugenio A. Veloso for providing comments on the earlier version of the manuscript. We are grateful to Dr Peter Milligan and his colleagues in Geoscience Australia for their dedication in conducting the Australia Wide Airborne Geophysical Surveys (AWAGS) and making the data available. DR also thanks Peter Milligan for his invitation to Geoscience Australia to discuss the AWAGS and determinations of Australian Curie depths. This study benefitted from the research carried under the US NSF grant EAR-1246921 and DR's participation in this study was made possible through NASA awards NNX16AN51G and 80NSSC19K0014. We are thankful to Dr Chun-Feng Li and Richard Chopping for sharing their DBMS results of Australia. The GMT (Generic Mapping Tool) system (Wessel *et al.* 2013) was used to prepare Figs 1, 2, 4, 7 and 8. The public domain data of aeromagnetic (http://www.geoscience.gov.au/gadds/), Moho depth (http://rses.anu.edu.au/seismology/AuSREM/Downloads/) and heat flow (https://data.gov.au/dataset/heat-flow-determinations-for-the-australian-continent-release-5) used for the study. We are thankful to Prof Richard Holme, Editor, other editors and two anonymous reviewers for their thoughtful comments on our manuscript which helped us in improving the manuscript. ARB is supported by CSIR-National Geophysical Research Institute main lab project MLP-6405. RK is thankful for receiving research support from Indian Institute of Geomagnetism Mumbai (IIGM), Department of Science and Technology, India.

REFERENCES

Aitken, A.R.A. & Betts, P.G., 2008. High-resolution aeromagnetic data over central Australia assist Grenville-era (1300-1100 Ma) Rodinia reconstructions, *Geophys. Res. Lett.,* **35,** L01306.

Aitken, A.R.A., Betts, P.G., Weinberg, R.F. & Gray, D., 2009. Constrained potential field modeling of the crustal architecture of the Musgrave Province in central Australia: evidence for lithospheric strengthening due to crust-mantle boundary uplift. *J. geophys. Res.,* **114**(12), art. no. B12405, doi:10.1029/2008JB006194.

Aitken, A.R.A., 2010. Moho geometry gravity inversion experiment (MoGGIE): a refined model of the Australian Moho, and its tectonic and isostatic implications, *Earth planet. Sci. Lett.,* **297,** 71–83.

Aitken, A.R.A., Salmon., M. & Kennett, B.L.N., 2013. Australia's Moho: a test of the usefulness of gravity modeling for the determination of Moho depth, *Tectonophysics,* **609,** 468–479.

Allen, P.A., Eriksson, P.G., Alkmin, F.F., Betts, P.G., Catuneanu, O., Mazumder, R., Meng, Q. & Young, G.M., 2015. Classification of basins, with special reference to Proterozoic examples, in *Precambrian Basins of India: Stratigraphic and Tectonic Context,* Vol. **43,** pp. 5–28, eds Mazumder, R. & Eriksson, P.G., Geological Society.

Artemieva, I.M., 2006. Global 1° × 1° thermal model TC1 for the continental lithosphere: implications for lithosphere secular evolution, *Tectonophysics,* **416,** 245–277.

Bansal, A.R., Dimri, V.P., Kumar, R. & Anand, S.P., 2016. Curie Depth estimation from aeromagnetic for fractal distribution of sources, in *Fractal Solutions for Understanding Complex System in Earth Sciences,* pp. 19–31, ed. Dimri, V.P., Springer Earth System Sciences.

Bansal, A.R., Gabriel, G., Dimri, V.P. & Krawczyk, C.M., 2011. Estimation of the depth to the bottom of magnetic sources by a modified centroid method for fractal distribution of sources: an application to aeromagnetic data in Germany, *Geophysics,* **76,** L11–L22.

Barley, M.E., Loader, S.E. & Mcnaughton, N.J., 1998. 3430–3417 calcalkaline volcanism in the McPhee Dome and Kelly Belt, and growth of the eastern Pilbara Craton, *Precambrian Res.,* **88,** 3–23.

Beardsmore, G., 2004. The influence of basement on surface heat flow in the Cooper Basin, *Explor. Geophys.,* **35,** 223–235.

Betts, P.G., Giles, D., Lister, G.S. & Frick, L.R., 2002. Evolution of the Australian Lithosphere, *Aust. J. Earth Sci.,* **49,** 661–692.

Betts, P.G., Giles, D., Mark, G., Lister, G.S., Goleby, B.R. & Aillères, L., 2006. Synthesis of the Proterozoic evolution of the Mt. Isa Inlier, *Aust. J. Earth Sci,* **53,** 187–211.

Betts, P.G. & Giles, D., 2006. The 1800-1100 Ma tectonic evolution of Australia, *Precambrian Res.,* **144,** 92–125.

Betts, P.G., Giles, D. & Schaefer, B.F., 2008. Comparing 1800-1600 Ma accretionary and basin processes in Australia and Laurentia: Possible geographic connections in Columbia, *Precambrian Res.,* **166,** 81–92.

Betts, P.G. *et al.*, 2016. Australia and Nuna, *Geol. Soc. Spec. Publ.,* **424,** 47–81.

Bhattacharyya, B.K. & Leu, L.K., 1975. Analysis of magnetic anomalies over Yellowstone National Park: mapping of Curie point isothermal surface for geothermal reconnaissance, *J. geophys. Res.,* **80,** 4461–4465.

Bhattacharyya, B.K. & Leu, L.K., 1977. Spectral analysis of gravity and magnetic anomalies due to rectangular prismatic bodies, *Geophysics,* **42,** 41–50.

Blaikie, T.N., Betts, P.G., Armit, R.J. & Ailleres, L. 2017. The ca. 1740–1710 Ma Leichhardt Event: inversion of a continental rift and revision of the tectonic evolution of the North Australian Craton. *Precambrian Res.,* **292,** 75–92.

Blakely, R.J., Brocher, T.M. & Wells, R.E., 2005. Subduction-zone magnetic anomalies and implications for hydrated forearc mantle, *Geology,* **33**(6), 445–448.

Blakely, R.J., 1995. *Potential Theory in Gravity & Magnetic Applications,* Cambridge Univ. Press.

Bouligand, C., Glen, J.M.G. & Blakely, R.J., 2009. Mapping Curie temperature depth in the western United States with a fractal model for crustal magnetization, *J. geophys. Res.,* **114,** B11104, doi:10.1029/2009JB006494.

Cawood, P.A., 2005. Terra Australia Orogen: Rodinia breakup and development of the Pacific and Iapetus margins of Gondwana during the Neoproterozoic and Paleozoic, *Earth Sci. Rev.,* **69,** 249–279.

Cawood, P. & Korsch, R.J., 2008. Assembling Australia: Proterozoic building of a continent, *Precambrian Res.,* **166,** 1–38.

Cawood, P.A., Pisarevsky, S.A. & Leitch, E.C., 2011. Unraveling the New England orocline, east Gondwana accretionary margin, *Tectonics,* **30,** TC5002, doi:10.1029/2011TC002864.

Cayley, R.A. *et al.*, 2011. Crustal architecture of central Victoria: results from the 2006 deep crustal reflection seismic survey, *Aust. J. Earth Sci.,* **58,** 113–156.

Chopping, R. & Kennett, B.L.N., 2015. Maximum depth of magnetization of Australia, its uncertainty and implications for Curie depth, *Geo Res. J.,* **7,** 70–77.

Clitheroe, G., Gundmundsson, O. & Kennett, B.L.N., 2000. The crustal thickness of Australia, *J. geophys. Res.,* **105,** 13 697–13 713.

Collins, A.S., 2002. Nature of extensional accretionary orogens, *Tectonics,* **21,** 1024, TC001272.

Collins, W.J. & Richards, S.W., 2008. Geodynamic significance of 'post-collisional' S-type granites in circum-Pacific orogens, *Geology,* **36,** 559–562

Conor, C.H.H. & Preiss, W.V., 2008. Understanding the 1720–1640 Ma Palaeoproterozoic Willyama Supergroup, Curnamona Province, south-eastern Australia: implications for tectonics, basin evolution and ore genesis, *Precambrian Res.,* **166,** 297–317.

Cull, J.P., 1982. An appraisal of Australian heat flow data, *BMR J. Aust. Geol. Geophys.,* **7,** 11–21.

Cull, J.P., 1991. Heat flow and regional geophysics in Australia, in *Terrestrial Heat Flow and Lithospheric Structure,* pp. 486–500, eds Cermak, V. & Rybach, L., Springer-Verlag.

Cull, J.P. & Beardsmore, G.R., 1992. Statistical methods for estimates of heat flow in Australia, *Explor. Geophys.,* **23,** 83–86.

Davies, D.R., Rawlinson, N., Iaffaldano, G. & Campbell, I.H., 2015. Lithospheric controls on magma composition along Earth's longest continental hotspot track, *Nature,* **525**(7570), 511–514.

Debayle, E., Kennett, B. & Priestley, K., 2005. Global azimuthal seismic anisotropy and the unique plate-motion deformation of Australia, *Nature,* **433,** 509–512.

De Ritis, R., Ravat, D., Ventura, G. & Chiappini, M., 2013. Curie isotherm depth from aeromagnetic data constraining shallow heat source depths in the central Aeolian Ridge (Southern Tyrrhenian Sea, Italy), *Bull. Volcanol.,* **75,** 710.

Dunlop, D.J. & Ozdemir, O., 1997. *Rock Magnetism. Fundamentals and Frontiers, Cambridge Studies in Magnetism Series,* Cambridge Univ. Press.

Fedi, M., Quarta, T. & Santis, A.D., 1997. Inherent power-law behavior of magnetic field power spectra from a Spector and Grant ensemble, *Geophysics,* **62,** 1143–1150.

Fergusson, C.L., Offler, R. & Green, T.J., 2009. Late Neoproterozoic passive margin of East Gondwana: geochemical constraints from the Anakie Inlier, central Queensland, Australia, *Precambrian Res.,* **168,** 301–312.

Fergusson, C.L. & Henderson, R.A., 2015. Early Palaeozoic continental growth in the Tasmanides of northeast Gondwana and its implications for Rodinia assembly and rifting, *Gondwana Res.,* **28,** 933–953.

Fergusson, C.L., Henderson, R.A. & Offler, R., 2017. Late Neoproterozoic to Early Mesozoic Sedimentary Rocks of the Tasmanides, Eastern Australia: provenance switching associated with development of the East Gondwana active margin, in *Sediment Provenance,* pp. 325–369, ed. Mazumder, R., Elsevier.

Ferré, E.C., Kupenko, I., Martín-Hernández, F., Ravat, D. & Sanchez-Valle, C., 2020, Magnetic sources in the Earth's mantle, *Nat. Rev. Earth Environ.,* **2,** 59–69.

Ferré, E.C., Friedman, S.A., Hernandez, F.M., Feinberg, J.M., Till, J.L., Ionov, D.A. & Conder, J.A., 2014. Eight good reasons why the uppermost mantle could be magnetic, *Tectonophysics,* **624–625,** 3–14.

Fishwick, S., Heintz, M., Kennett, B.L.N., Reading, A.M. & Yoshizawa, K., 2008. Steps in lithospheric thickness within eastern Australia, evidence from surface wave tomography, *Tectonics,* **27,** TC4009.

Foden, J., Elburg, M.A., Dougherty-Page, J. & Burtt, A., 2006. The timing and duration of the Delamerian orogeny: correlation with the Ross Orogen and implications for Gondwana assembly, *J. Geol.,* **114,** 189–210.

Gerner, E. & Holgate, F., 2010. *Oztemp interpreted temperature at 5 km depth*, Canberra: Digital data, Geoscience Australia, GEOCAT reference 71143.

Gibson, G.M., Rubenach, M.J., Neumann, N.L., Southgate, P.N. & Hutton, L.J., 2008. Syn- and post-extensional tectonic activity in the Palaeoproterozoic sequences of Broken Hill and Mount Isa and its bearing on reconstructions of Rodinia, *Precambrian Res.,* **166,** 350–369.

Gibson, G.M., Champion, D.C., Withnall, I.W., Neumann, N.L. & Hutton, L.J., 2018. Assembly and breakup of the Nuna supercontinent: geodynamic constraints from 1800 to 1600 Ma sedimentary basins and basaltic magmatism in northern Australia, *Precambrian Res.,* **313,** 148–169,

Gibson, G.M. & Edwards, S., 2020. Basin inversion and structural architecture as constraints on fluid flow and Pb-Zn mineralization in the Paleo-Mesoproterozoic sedimentary sequences of northern Australia, *Solid Earth,* **11,** 1205–1226.

Giles, D., Betts, P.G. & Lister, G.S., 2004. 1.8–1.5-Ga links between the North and South Australian Cratons and the Early–Middle Proterozoic configuration of Australia, *Tectonophysics,* **380,** 27–41.

Glen, R.A., 2005. *The Tasmanides of Eastern Australia,* Geological Society Special Publication, **246,** 23–96.

Goleby, B.R., Blewett, R.S., Korsch, R.J., Champion, D.C., Cassidy, K.F., Jones, L.E.A., Groenewald, P.B. & Henson, P., 2004. Deep seismic reflection profiling in the Archaean northeastern Yilgarn Craton, Western Australia: Implications for crustal architecture and mineral potential, *Tectonophysics,* **388,** 119–133.

Goleby, B.R., Shaw, R.D., Wright, C., Kennett, B.L.N. & Lambeck, K., 1989. Geophysical evidence for 'thick-skinned' crustal deformation in central Australia, *Nature,* **337,** 325–330.

Goleby, B.R., Kennertt, B.L.N., Wright, C., Shaw, R.D. & Lambeck, K., 1990, Seismic reflection profiling in the Proterozoic Arunta block, central Australia: processing for testing models of tectonic evolution, *Tectonophysics,* **173,** 257–268.

Guimaraes, S.N.P., Ravat, D. & Hamza, V.M., 2014. Combined use of the centroid and matched filtering spectral methods in determining thermomagnetic characteristics of the crust in the structural provinces of Central Brazil, *Tectonophysics,* **624–625,** 87–99.

Hand, M., Reid, A. & Jagodzinski, L., 2007. Tectonic framework and evolution of the Gawler craton, Southern Australia, *Econ. Geol.,* **102,** 1377–1313

Haggerty, S.E., 1978. Mineralogical constraints on Curie isotherms in deep crustal magnetic anomalies, *Geophys. Res. Lett.,* **5,** 105–108.

Holzrichter, N., Hackney, R. & Johnston, S., 2014. Crustal structure of the northern Perth basin, southwest margin of Australia: insights from the three-dimensional density models, *Geophys. J. Int.,* **196,** 204–217.

Housemann, G.A., Cull, J.P., Muir, P.M. & Paterson, H.L., 1989. Geothermal signatures and uranium ore deposits on the Stuart Shelf of South Australia, *Geophysics,* **54,** 158–170.

Jackson, M.J., Sweet, I.P. & Powell, T.G., 1988. Studies on petroleum geology and geochemistry, middle Proterozoic, McArthur Basin, northern Australia; Petroleum potential I, *APEA J.,* **28,** 283–302.

Jones, I. & Verdel, C., 2015. Basalt distribution and volume estimates of Cenozoic volcanism in the Bowen Basin region of eastern Australia: implications for a waning mantle plume, *Aust. J. Earth Sci.,* **62,** 255–263.

Kennett, B.L.N., Salmon, M. & Saygin, E., Aus Moho Working Group, 2011. Aus Moho: the variation of Moho depth in Australia, *Geophys. J. Int.,* **187,** 946–958.

Kirkby, A.L. & Gerner, E.J., 2013. *Heat Flow Determinations for the Australian Continent*, Release 5, Record 2013/34, Geoscience Australia, Canberra.

Kirkland, C.L. *et al.*, 2013. Constraints and deception in the isotopic record: the crustal evolution of the west Musgrave Province, central Australia, *Gondwana Res.,* **23,** 759–781.

Korsch, R.J., Totterdell, J.M., Cathro, D.L. & Nicoll, M.G., 2009. Early Permian east Australian rift system, *Aust. J. Earth Sci,* **56,** 381–400.

Kumar, R., Bansal, A.R., Anand, S.P., Rao, V.K. & Singh, U.K., 2018, Mapping of magnetic basement in Central India from aeromagnetic data for scaling geology, *Geophys. Prospect.,* **66,** 226–239.

Kumar, R., Bansal, A.R. & Ghods, A., 2020. Estimation of depth to bottom of magnetic sources using spectral methods: application on Iran's aeromagnetic data, *J. geophys. Res.,* **125,** doi:10.1029/2019JB018119.

Lambeck, K., 1983. Structure and evolution of the intracratonic basins of central Australia. *Geophys. J. R. astr. Soc.,* **74,** 843–886.

Lambeck, K., Burgess, G. & Shaw, R.D., 1988. Teleseismic travel-time anomalies and deep crustal structure in central Australia. *Geophys. J. R. astr. Soc.,* **94,** 105–124.

Li, C-F., Wang, J., Lin, J. & Wang, T., 2013. Thermal evolution of the north Atlantic lithosphere: new constraints from magnetic anomaly inversion with a fractal magnetization model, *Geochem. Geophys. Geosyst.,* **12,** 5078–5105.

Li, C-F., Lu, Y. & Wang, J., 2017. A global reference model of Curie-point depths based on EMAG2, *Scientific Reports, Nature,* **7,** 45129.

Maidment, D.W., Williams, I.S. & Hand, M., 2007. Testing long-term patterns of basin sedimentation by detrital zircon geochronology, Centralian Superbasin, Australia, *Basin Res.,* **19,** 335–360.

Martin, D. McB., Li, Z.X., Nemchin, A.A. & Powell, C. McA., 1998. A pre-2.2 Ga age for giant hematite ores of the Hamersley Province, Australia? *Econ. Geol.,* **93,** 1084–1090.

Maus, S. & Dimri, V.P., 1994. Scaling properties of potential fields due to scaling sources. *Geophys. Res. Lett.,* **21**(10), 891–894.

Maus, S. & Dimri, V.P., 1996. Depth estimation from the scaling power spectrum of potential fields, *Geophys. J. Int.,* **124,** 113–120.

Maus, S., Gordon, D. & Fairhead, J.D., 1997. Curie temperature depth estimation using a self-similar magnetization model, *Geophys. J. Int.,* **129,** 163–168.

McLaren, S., Sandiford, M., Hand, M., Neumann, N., Wyborn, L. & Bastrakova, I., 2003. The hot southern continent: heat flow and heat production in Australian Proterozoic terranes, *Geol. Soc. Am. Spec. Publ.,* **372,** 157–167.

McLaren, S., Sandiford, M., Powell, R., Neumann, N. & Woodhead, J., 2006. Palaeozoic Intraplate Crustal Anatexis in the Mount Painter Province, South Australia: timing, thermal budgets and the role of crustal heat production, *J. Petrol.,* **47,** 2281–2302.

Meixner, A.J., Kirkby, A.L. & Horspool, N., 2014. Using constrained gravity inversions to identify high-heat-producing granites beneath thick sedimentary cover in the Cooper Basin region of central Australia, *Geothermics,* **51,** 483–495.

Meixner, A.J., Kirkby, A.L., Lescinsky, D.T. & Horspool, N., 2012. The Cooper Basin 3D Map Version 2: thermal modelling and temperature uncertainty, Geoscience Australia Record 60.

Mengel, K. & Kernt, H., 1992. Evolution of petrological and seismic Moho implications for the continental crust-mantle boundary, *Terra Nova,* **4,** 109–116.

Middleton, M.F., 2013. Radiogenic heat generation in the Darling range, Western Australia, *Explor. Geophys.,* **44,** 206–214.

Milligan, P.R., Minty, B.R.S., Richardson, M. & Franklin, R., 2009. The Australia-wide Airborne Geophysical Survey – accurate continental magnetic coverage, *Preview,* **138,** 70.

Milligan, P.R., Franklin, R., Minty, B.R.S., Richardson, L.M. & Percival, P.J., 2010. *Magnetic Anomaly Map of Australia*, 1:5 000 000 scale, Geoscience Australia, Canberra.

Morrissey, L.J., Hand, M., Raimondo, T. & Kelsey, D.E., 2014. Long-lived high-T, low-P granulite facies metamorphism in the Arunta region, central Australia, *J. Metamorph. Geol.,* **32,** 25–47.

Moresi, L., Betts, P.G., Miller, M.S. & Cayley, R.A., 2014. Dynamics of continental accretion *Nature,* **508,** 245–248.

Morgan, P., 1985. Crustal radiogenic heat production and the selective survival of ancient continental crust, *J. geophys. Res.,* **90,** C561–C570.

Myers, J.S., Shaw, R.D. & Tyler, I.M., 1996. Tectonic evolution of Proterozoic Australia, *Tectonics,* **15,** 1431–1446.

Neumann, N.L., Southgate, P.N. & Gibson, G.M., 2009. Defining unconformities in Proterozoic sedimentary basins using detrital geochronology and basin analysis-an example from the Mount Isa Inlier, Australia, *Precambrian Res.,* **168,** 149–166.

Neumann, N., Sandiford, M. & Foden, J., 2000. Regional geochemistry and continental heat flow: implications for the origin of the South Australia heat flow anomaly, *Earth planet. Sci. Lett.,* **183,** 107–120.

Nordsvan, A.R., Collins, W.J., Li, Z.X., Spencer, C.J., Pourteau, A., Withnall, I.W., Betts, P.G. & Volante, S., 2018. Laurentian crust in northeast Australia: implications for the assembly of the supercontinent Nuna, *Geology,* **46,** 251–254.

Okubo, Y., Graf, R.J., Hansen, R.O., Ogawa, K. & Tsu, H., 1985. Curie point depths of the island of Kyushu and surrounding area, Japan, *Geophysics,* **50,** 481–489.

Olsen, N., Ravat, D., Finlay, C.C. & Kother, L.K., 2017. LCS-1: a high-resolution global model of the lithospheric magnetic field derived from CHAMP and Swarm satellite observations, *Geophys. J. Int,* **211,** 1461–1477.

Percival, P.J., 2014. *Index of Airborne Geophysical Surveys (Fourteenth Edition),* Geoscience Australia, Record, 2014/014.

Pilkington, M. & Todoeschuck, J.P., 1993. Fractal magnetization of continental crust, *Geophys. Res. Lett.,* **20,** 627–630.

Pilkington, M. & Todoeschuck, J.P., 2004. Power-law scaling behavior of crustal density and gravity, *Geophys. Res. Lett.,* **31,** L09606, doi:10.1029/2004GL019883.

Pirajno, F. & Hoatson, D.M., 2012. A review of Australia's large igneous provinces and associated mineral systems: implications for mantle dynamics through geological time, *Ore Geol. Rev.,* **48,** 2–54.

Powell, C. McA., Oliver, N.H.S., Li, Z.X., Martin, D. McB. & Ronaszeki, J., 1999. Syn-orogenic hydrothermal origin for giant Hamersley iron oxide ore bodies, *Geology,* **27,** 175–178.

Powell, C. McA., Preiss, W.V., Gatehouse, C.G., Krapez, B. & Li, Z.X., 1994. South Australian record of a Rodinian epicontinental basin and its mid-neoproterozoic breakup (∼700 Ma) to form the Palaeo-Pacific Ocean, *Tectonophysics,* **237,** 113–140.

Preiss, W.V., 2000. The Adelaide Geosyncline of South Australia and its significance in Neoproterozoic continental reconstruction, *Precambrian Res.,* **100,** 21–63.

Ravat, D., Pignatelli, A., Nicolosi, I. & Chiappini, M., 2007. A study of spectral methods of estimating the depth to the bottom of magnetic sources from near-surface magnetic anomaly data, *Geophys. J. Int.,* **169,** 421–434.

Ravat, D., Morgan, P. & Lowry, A.R., 2016. Geotherms from the temperature-depth constrained solutions of 1-D steady-state heat flow equation, *Geosphere,* **12,** 1187–1197.

Ravat, D., 2019. The Moho is not the magnetization limit: evidence from North American magnetic anomalies from the spectral multi-defractal method, in *American Geophysical Union, Fall Meeting 2019*, abstract #GP23A-05GP23A-05.

Reid, A., Hand, M., Jagodzinski, E., Kelsey, D. & Pearson, N.J., 2008. Palaeoproterozoic orogenesis within the southeastern Gawler Craton, South Australia, *Aust. J. Earth Sci.,* **55,** 449–471.

Rosenbaum, G., 2018. The Tasmanides: Phanerozoic tectonic evolution of Eastern Australia, *Annu. Rev. Earth planet. Sci.,* **46,** 291–325.

Ross, H.E., Blakely, R.J. & Zoback, M.D., 2006. Testing the use of aeromagnetic data for the determination of Curie depth in California, *Geophysics,* **71,** L51–L59.

Salem, A., Green, C., Ravat, D., Singh, H.K., East, P., Fairhead, J.D., Morgen, S. & Biegert, E., 2014. Depth to Curie temperature across the central Red Sea from magnetic data using the de-fractal method, *Tectonophysics,* **624–625,** 75–86.

Salmon, M., Kennett, B.L.N., Stern, T. & Aitken, A.R.A., 2013. The Moho in Australia and New Zealand, *Tectonophysics,* **609,** 288–298.

Sippl, C., Brisbout, L., Spaggiari, C.V., Gessner, K., Tkalc˘ic´, H., Kennett, B.L.N. & Murdie, R., 2017. Crustal structure of a Proterozoic craton boundary: East Albany-Fraser Orogen, Western Australia, imaged with passive seismic and gravity anomaly data, *Precambrian Res.,* **296,** 78–92.

Smithies, R.H. & Bagas, L., 1997. High pressure amphibolite-granulite facies metamorphism in the Paleoproterozoic Rudall Complex, central Western Australia, *Precambrian Res.,* **83,** 243–265.

Southgate, P.N. *et al.*, 2000. Chronostratigraph basin framework for Palaeoproterozoic rocks (1730–1575 Ma) in northern Australia and implications for base-metal mineralization, *Aust. J. Earth Sci.,* **47,** 461–483.

Spaggiari, C.V., Kirkland, C.L., Smithies, R. & Wingate, M., 2014. Tectonic links between Proterozoic sedimentary cycles, basin formation and magmatism in the Albany-Fraser Orogen, Western Australia, *Geol. Surv. Western Aust., Rep.,* **133,** 1–63.

Spaggiari, C.V., Kirkland, C.L., Smithies, R.H., Wingate, M.T.D. & Belousova, E.A., 2015. Transformation of an Archean craton margin during Proterozoic basin formation and magmatism: The Albany-Fraser Orogen, Western Australia, *Precambrian Res.,* **266,** 440–466.

Spampinato, G.P.T., Ailleres, L., Betts, P.G. & Armit, R.J., 2015a. Imaging the basement architecture across the Cork Fault in Queensland using magnetic and gravity data, *Precambrian Res.,* **264,** 63–81.

Spampinato, G.P.T., Betts, P.G., Ailleres, L. & Armit, R.J., 2015b. Early tectonic evolution of the Thomson Orogen in Queensland inferred from constrained magnetic and gravity data, *Tectonophysics,* **651** 99–120.

Stewart, J.R. & Betts, P.G., 2010. Implications for Proterozoic plate margin evolution from geophysical analysis and crustal-scale modeling within the western Gawler Craton, Australia, *Tectonophysics,* **483**(1-2), 151–177.

Stewart, A.J., Raymond, O.L., Totterdell, J.M., Zhang, W. & Gallagher, R., 2013. Australian Geological Provinces 2013.01 edition, Digital Dataset, Geoscience Australia, Commonwealth of Australia, Canberra. http://www.ga.gov.au.

Swain, G.M., Barovich, K., Hand, M., Ferris, G. & Schwarz, M., 2008. Petrogenesis of the St Peter Suite, southern Australia: arc magmatism and Proterozoic crustal growth of the South Australian Craton, *Precambrian Res.,* **166,** 283–296

Tanaka, A., Okubo, Y. & Matsubayashi, O., 1999. Curie point depth based on spectrum analysis of the magnetic anomaly data in East and Southeast Asia, *Tectonophysics,* **306,** 461–470.

Toft, P.B. & Haggerty, S.E., 1988. Limiting depth of magnetization in cratonic lithosphere. *Geophys. Res. Lett.,* **15,** 530–533.

Vervelidou, F. & Thébault, E., 2015. Global maps of the magnetic thickness and magnetization of the Earth's lithosphere*, Earth Planets Space,* **67,** 173.

Vitorello, I. & Pollack, H.N., 1980. On the variation of continental heat flow with age and the thermal evolution of continents, *J. geophys. Res.,* **85,** 983–995.

Wade, B.P., Barovich, K.M., Hand, M., Scrimgeour, I.R. & Close, D.F., 2006. Evidence for Early Mesoproterozoic arc magmatism in the Musgrave Block, central Australia: implications for Proterozoic crustal growth and tectonic reconstructions of Australia, *J. Geol.,* **114,** 43–63.

Wasilewski, P.J., Thomas, H.H. & Mayhew, M.A., 1979. The Moho as magnetic boundary, *Geophys. Res. Lett.,* **6,** 541–544.

Wasilewski, P. & Mayhew, M., 1992. The Moho as magnetic boundary revisited, *Geophys. Res. Lett.,* **19,** 2259–2262.

Wessel, P., Smith, W.H.F., Scharroo, R., Luis, J. & Wobbe, F., 2013. Generic mapping tools: improved version released, *EOS, Trans. Am. geophys. Un.,* **94**(45), 409–410.

Withnall, I., Hutton, L.J., Armit, R., Betts, P.G., Blewett, R. & Champion, D.C., 2013. North Australian craton. Geology of Queensland, in *Geology of Queensland,* pp. 23–112, ed. Jell, P., Geological Survey of Queensland.